https://doi.org/10.5194/essd-2024-323
Preprint. Discussion started: 12 August 2024

Open Access Earth System Science Data Discussions

Annual mass changes for each glacier in the world from 1976 to 2023

Inés Dussaillant[1], Romain Hugonnet[2], Matthias Huss[3], Etienne Berthier[4], Jacqueline Bannwart[1], Frank Paul[1], Michael Zemp[1]

[1] Department of Geography, University of Zurich, Switzerland
[2] University of Washington, Civil and Environmental Engineering, Seattle, WA, USA
[3] Laboratory of Hydraulics, Hydrology and glaciology (VAW) ETH Zurich, Switzerland
[4] LEGOS, Université de Toulouse, CNES, CNRS, IRD, UPS, Toulouse, France

Correspondence to : Inés Dussaillant (ines.dussaillant@geo.uzh.ch)

Abstract. Glaciers, distinct from the Greenland and Antarctic ice sheets, play a crucial role in Earth's climate system by affecting global sea levels, freshwater availability, nutrient and energy budgets and regional climate patterns. Accurate measurements of glacier mass changes are needed to understand and project glacier evolution and its related impacts on the climate system. Two distinct methods allow to measure glacier mass changes at high spatial resolution. Remotely sensed surface elevation data provides volume change estimates over large glacierized regions for multi-annual to decadal time periods. Field glaciological measurements provide annually to seasonally resolved information on glacier mass change for a small sample of the world's glaciers. By combining the two methods we provide annual time series of individual glacier mass changes and related uncertainties spanning the hydrological years from 1976 to 2023. The per-glacier time series can then be seamlessly integrated into annually resolved global regular grids of glacier mass changes at user-specified spatial resolution. Our results undergo a leave-one-out cross-validation confirming uncertainty estimates at the glacier level to be in the conservative side. Our dataset provides a new baseline for future glacier change modelling assessments and their impact on the world's energy, water, and sea-level budget. The present annual mass change time-series for the individual glaciers and the derived global gridded annual mass change product at a spatial resolution of 0.5° latitude and longitude will be made available from the WGMS webpage. During the review process, the dataset is temporarily available from URL: https://user.geo.uzh.ch/idussa/Dussaillant_etal_ESSD_data/.

1 Introduction

Glacier monitoring has witnessed significant advancements since its beginning in the late 19th century with the use of both in-situ (glaciological) and remotely sensed (geodetic) methods to observe changes in glacier elevation, volume and mass (Zemp et al., 2015a; Thomson et al., 2021). The glaciological method provides detailed, annual to seasonally resolved insights into glacier mass change variations, reflecting the impact of prevalent atmospheric conditions correlated over several hundred kilometers (Letréguilly and Reynaud, 1990; Østrem and Brugman, 1991; Cogley and Adams, 1998; Oerlemans, 2001; Kaser et al., 2003; Cogley et al., 2011; Zemp et al., 2013, 2015, 2019; Braithwaite and Hughes, 2020; Fernández and Somos-

https://doi.org/10.5194/essd-2024-323
Preprint. Discussion started: 12 August 2024

Valenzuela, 2022). In-situ observations cover only a limited sample of the world's glaciers, representing less than 1% or approximately 500 glaciers. Thanks to the coordination of the World Glacier Monitoring Service (WGMS) and its global network of contributors, nearly all glacier regions are represented. These glaciological observations, while valuable, are subject to potential biases and often require validation or correction with high-resolution airborne geodetic surveys (Thibert et al., 2008; Thibert and Vincent, 2009; Zemp et al., 2013).

As a complement, the geodetic method using airborne and spaceborne sensors has become a powerful tool to measure glacier elevation changes over large glacierized areas with high accuracy for multiannual to decadal timeframes (Cogley et al., 2011). The digital elevation model (DEM) differencing technique, initially applied to DEMs derived from maps (Joerg and Zemp, 2014), aerial photographs (Finsterwalder, 1954; Thibert et al., 2008; Papasodoro et al., 2015; Belart et al., 2019, 2020) has evolved to include data from airborne Lidar (Echelmeyer et al., 1996; Abermann et al., 2010) spaceborne altimetry (Jakob and Gourmelen, 2023) and satellite derived DEMs (Toutin, 2001; Berthier et al., 2023). Advanced postprocessing techniques (Arendt, 2002; Hagg et al., 2004; Rolstad et al., 2009; Nuth and Kääb, 2011; Gardelle et al., 2013; Huss, 2013; Dehecq et al., 2016; McNabb et al., 2019; Hugonnet et al., 2022), supercomputing capabilities, and automated processing pipelines (Shean et al., 2016; Girod et al., 2017; Rupnik et al., 2017) have further enhanced this method. This progress has enabled the application of the geodetic method over entire mountain ranges (Brun et al., 2017; Braun et al., 2019; Dussaillant et al., 2019; Menounos et al., 2019; Shean et al., 2020) and even on a global scale (Hugonnet et al., 2021).

Various methods, or combination thereof, have been proposed to assess global glacier mass changes with the objective to quantify the contribution to global sea level rise and regional hydrology (Gardner et al., 2013; Wouters et al., 2019; Zemp et al., 2019; Hugonnet et al., 2021; Jakob and Gourmelen, 2023). Among these, the works of Zemp et al. (2019) and Hugonnet et al., (2021) stand out as the only global studies relying on high spatial resolution data, the later even able to resolve individual glacier changes. Zemp et al., (2019) combines the temporal variability of the glaciological observations with the long-term trends of the geodetic method available from the FoG database, capturing the annual variability of glacier mass changes for all 19 glacier regions (GTN-G, 2017) since the 1960s. While offering the advantages of annual resolution and the capacity to bring glacier observations back in time, the limited observational sample at the time of that study (only 9% of Earth's glacier by number) results in relatively high uncertainties, impacting the reliability of long-term trends, and evident during the more recent years when compared to Hugonnet et al., (2021). In contrast, the estimates by Hugonnet et al., (2021) provide nearly globally complete 20-year trends at the scale of individual glaciers, with uncertainties validated against independent high-resolution datasets. By leveraging the repeated acquisitions and global coverage of the Advanced Spaceborne and Thermal Emission and Reflection (ASTER) satellite optical stereo images (Raup et al., 2000), the assessment provides individual glacier elevation changes since year 2000 for nearly all glaciers worldwide (97.4% of inventoried glacier area (RGI Consortium, 2017)). Despite its strengths, this approach also has its limitations, including a relatively short observational period, and the

https://doi.org/10.5194/essd-2024-323
Preprint. Discussion started: 12 August 2024

inability of the geodetic method to capture annual glacier mass changes, mostly due to the high uncertainties of volume-to-mass density conversion factors for short timeframes (Huss, 2013).

The primary gap in global observation-based glacier change assessments remains therefore both on the quantification of global glacier ice changes prior to years 2000 but most importantly in understanding the spatial and temporal distribution of these changes. Thanks to the now almost complete coverage provided by Hugonnet et al. (2021) (covering 96% of the worlds glaciers) plus the various glacier elevation data available from the multiple local and regional geodetic glacier change assessments (covering a 17% of the worlds glaciers), a global-scale observation-based assessment of annually resolved glacier mass changes at a glacier-specific level has become feasible. Building upon the methodological foundations laid out in Zemp et al. (2019, 2020) prior work, we further developed the approach to integrate the temporal variability of glacier changes observed through the glaciological data with the long-term trends from the geodetic data sourced from the latest version of the Fluctuations of Glaciers (FoG) database (WGMS, 2024). We generate annual mass-change time-series since the hydrological year 1976 for each individual glacier across the globe cataloged by the Randolph Glacier Inventory (RGI-6.0, Pfeffer et al., 2014; RGI Consortium, 2017).

This novel observation-based glacier mass change assessment integrates the advantages of previous assessments, demonstrating significant strengths and clarifying its limitations. Our methodology performs well in regions with diverse, sufficient, continuous, and temporally well-represented observations, crucial for accurately reconstructing annual glacier change variability and multi-period trend calibration. We provide five decades of global glacier mass changes with high temporal and spatial resolution, correcting biases in long-term trends, and enhancing accuracy while reducing regional and global uncertainties. Validated through a leave-one-out cross-validation exercise, the dataset captures the interannual variability of glacier changes with realistic and robust uncertainty assessments, considering spatial correlations from both geodetic (related to elevation change and density transformation) and glaciological sample errors (related to glacier interannual variability). The dataset's versatility is a major asset, enabling detailed analysis of spatial and temporal glacier changes at various scales, from individual glaciers to global assessments. This comprehensive dataset facilitates detailed analyses of spatial and temporal glacier changes at multiple scales, from individual glaciers to global products.

2. Data and Methods

2.1 Input Datasets

2.1.1. Glacier inventories

We use the digital glacier outlines from the Randolph Glacier Inventory 6.0 (RGI Consortium, 2017) to spatially locate glaciers, measure their area and distribute the FoG observations on individual glaciers. This globally complete inventory of glacier outlines represents their area as it was near the beginning of the 21st century. RGI version 6.0 has been preferred to the most

https://doi.org/10.5194/essd-2024-323
Preprint. Discussion started: 12 August 2024

recent version 7.0 for two reasons: first, because FoG glacier elevation change observations are available only for version 6.0 and second, for comparison with previous observation based global assessments using this version. RGI outlines are available through the RGI online portal (DOI: 10.7265/N5-RGI-60) and the Global Land Ice Measurements from Space initiative (GLIMS, DOI: 10.7265/N5V98602). Due to the high number of incorrectly mapped glaciers in the RGI 6.0 Caucasus and Middle East region (region 12), the Hugonnet et al. (2021) geodetic observations were calculated using the latest GLIMS outlines available (Tielidze and Wheate, 2018). The former inventory is also used in this study for consistency. For the Greenland Periphery (region 5), we did not include glaciers strongly connected to the ice sheet (RGI 6.0 connectivity level 2). To spatially constrain glaciers within the world's climatic regions we use the 19 first-order glacier regions as defined by the Global Terrestrial Network for Glaciers (GTN-G, 2017) illustrated in Fig. 1. Glacier regions are implemented directly in the RGI dataset and are accessible via the same DOI. The location of the glacier and region outlines used in this study is represented in Fig. 1. The full regional hypsometric coverage is illustrated in grey bars in Fig. 1.

2.1.2 Glacier elevation and mass change observations

We use the annual mass change observations from the glaciological method and multiannual trends of elevation changes derived from the geodetic method as available from the latest update of the Fluctuations of Glaciers database (FoG). These glacier change observations are collected by the WGMS in annual calls-for-data through a worldwide network of national correspondents and principal investigators. After integration of the new, homogenized and corrected observations, a new FoG database version is released. Updated versions of the FoG database can be accessed via the WGMS online portal (https://wgms.ch/data_databaseversions/). Results presented here use version WGMS (2024) accessible through: https://doi.org/10.5904/wgms-fog-2024-01. The almost complete observational coverage of the latest FoG database version WGMS (2024) is depicted in Fig. 1, with the geodetic sample covering 96% of all the world's glaciers throughout their full hypsometry. The key characteristics of glacier mass and elevation change observations are summarized in Table 1. For more details on the specific input data, auxiliary data, retrieval algorithms and uncertainty estimation of the independent FoG glacier elevation and mass change observations please refer to (WGMS, 2024). More details on the glaciological method can be found in Østrem and Brugman (1991), Kaser et al. (2003) and Zemp et al. (2013, 2015). For the geodetic method and its error sources see WMO (2023) and about measuring glacier mass changes from space, see Berthier et al. (2023).

Table 1: Key characteristics of glacier elevation and mass change observations used in this study as available from the Fluctuations of Glaciers database (WGMS 2024)

	Glacier elevation change	Glacier mass change
Symbol	$\frac{dh}{dt}$	B_{glac}
Method	Geodetic method DEM differencing	Glaciological method

https://doi.org/10.5194/essd-2024-323
Preprint. Discussion started: 12 August 2024

Platform	In-situ, airborne, spaceborne	In-situ
Spatial resolution	Glacier-wide average from DEMs of meter to decameter pixel size	Glacier-wide average from interpolated point measurements
Spatial coverage	Worldwide (208,000 glaciers)	Worldwide (500 glaciers)
Temporal resolution	Multi-annual to decadal	Seasonal to annual
Temporal coverage	Start dates since early 20th century (vary by region) until present	Start dates between 1915-1976 (vary by region) until present
Unit	meter (m)	meter water equivalent (m w.e.)

https://doi.org/10.5194/essd-2024-323
Preprint. Discussion started: 12 August 2024

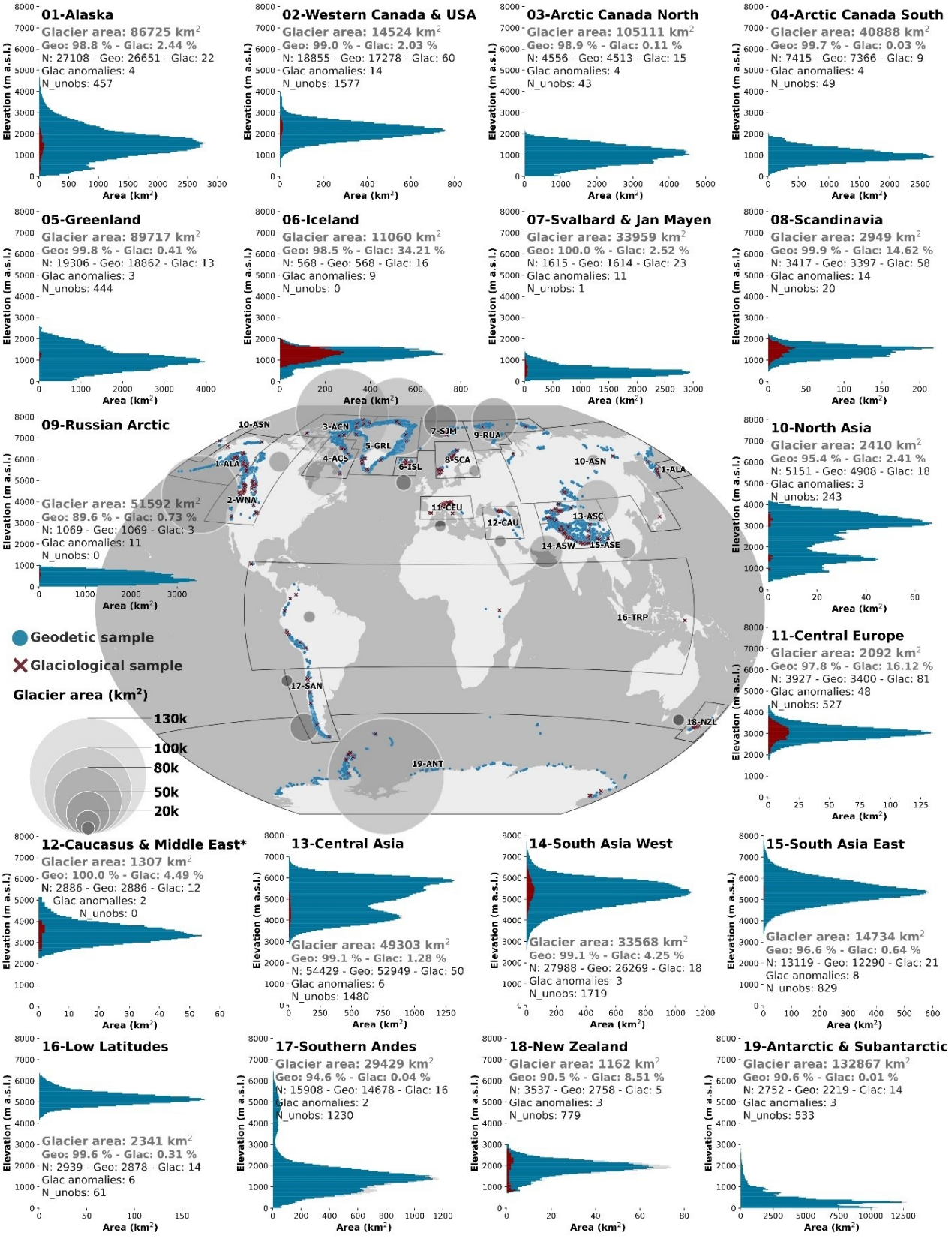

https://doi.org/10.5194/essd-2024-323
Preprint. Discussion started: 12 August 2024

Figure 1: Spatial and hypsometric coverage of glaciological and geodetic observations for each of the 19 first-order regions. Glacier hypsometry from RGI 6.0 (grey) is overlaid with glacier hypsometry of the geodetic elevation changes (Geo, blue) and the glaciological (Glac, red) samples used in this study. Values for the glacier area and total number (N) of glaciers are given for each region together with the respective percentage area covered, the number of observed and unobserved glaciers (N_unobs). The number of valid glacier anomalies (Glac anomalies) available are also noted per region.

* Tielidze and Wheate (2018) inventory available from GLIMS used

** Glaciers strongly connected to the ice sheet are not included

2.2 Methods

To prepare the data for the main processing, glacier-wide records with available mass and elevation change observations identified by a WGMS-Id are selected from the FoG database and related to their corresponding RGI outline identifier (RGIId) using a WGMS-Id to RGIId link-up table. We exclude geodetic records with survey periods shorter than five years in view of their large uncertainty for the density conversion (Huss, 2013). For simplicity, throughout this work hydrological years are represented as the last year of the hydrological cycle (e.g. 1976) starting on the 1st October to 30th September in the Northern Hemisphere, and from 1st April of the previous year (e.g. 1975) to 31st March of the year (e.g. 1976) in the Southern Hemisphere. For the Low Latitudes region, we assume the hydrological year to be equal to the calendar year from 1st January to 31st December.

Our processing algorithm is summarized in four key steps represented in Fig. 2. First, focusing on a specific glacier in the RGI-6.0 inventory (Fig. 2a), we estimate the detrended temporal variability of annual mass change for the glacier, referred here as the glacier mean annual anomaly, by extracting it from the interannual variability of nearby glaciological time series (Fig. 2b). Secondly, we calibrate the mean annual anomaly to the long-term trends from the geodetic sample available for the respective glacier (Fig. 2c). Third, we integrate all these calibrated time series into a single, area-weighted average, producing a data-fused annual mass change time series unique for every individual glacier (Fig. 2d).

https://doi.org/10.5194/essd-2024-323
Preprint. Discussion started: 12 August 2024

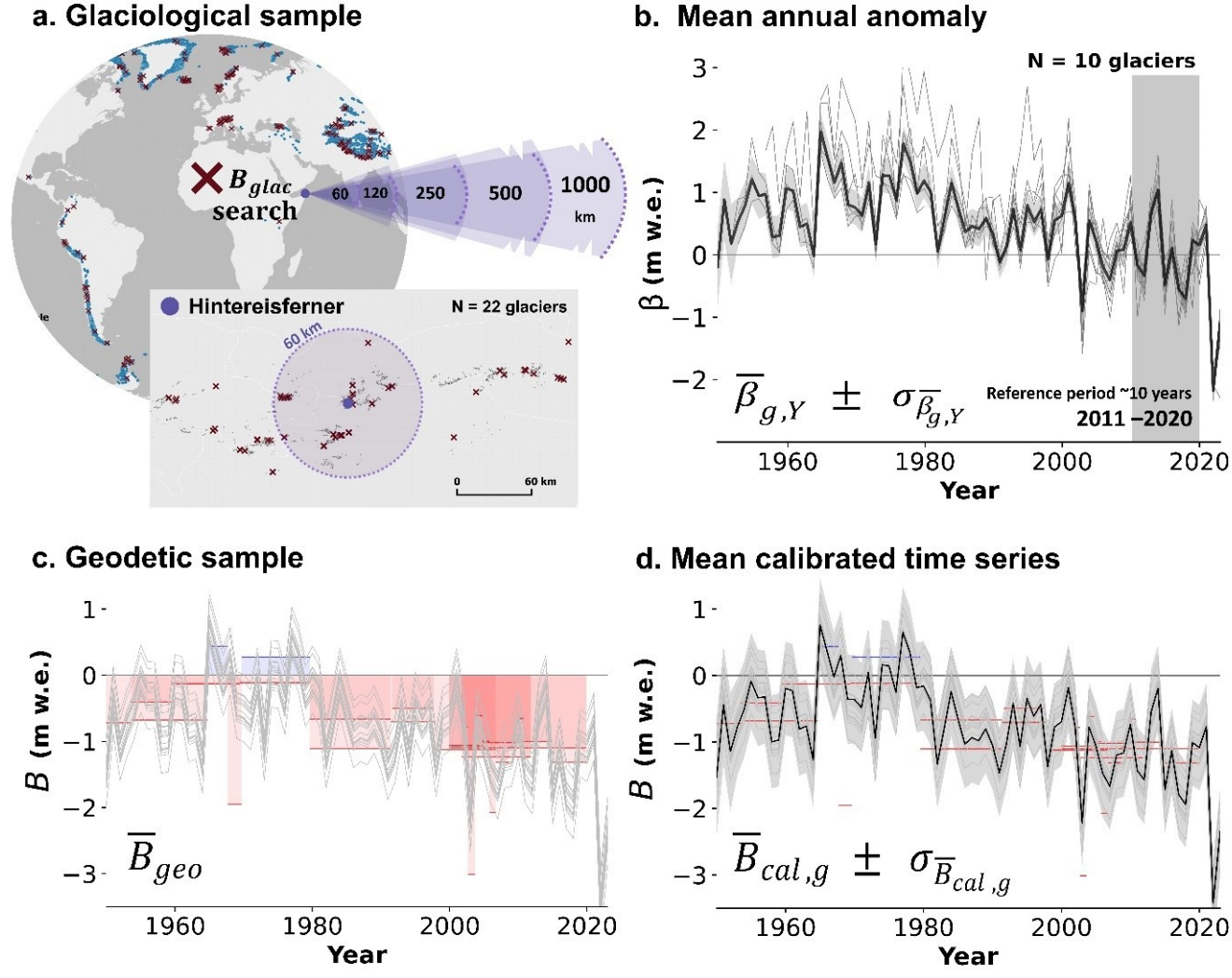

150 **Figure 2: Methodological steps illustrated at Hintereisferner, Central Europe.** (a) Spatial-distance search. Purple point shows the location of Hintereisferner, red crosses depict nearby glaciers with available glaciological observations. Within the first distance step of 60 km, 22 glaciers with glaciological observations are located. (b) Hintereisferner mean annual-anomaly. Grey lines correspond to the spatially-selected individual glacier anomalies, only 10 glaciers with anomalies over the reference period. (c) Calibration of the mean annual-anomaly over Hintereisferner geodetic mass change observations (Red and blue lines). Grey lines correspond to the individual calibrated time series
155 for each geodetic mass change observation (longer or equal to 5 years). (d) Hintereisferner mean calibrated mass change time series (black line) and uncertainty (grey).

https://doi.org/10.5194/essd-2024-323
Preprint. Discussion started: 12 August 2024


Open Access Earth System Science Data Discussions

2.2.1 Computing the mean annual anomaly from the neighboring glaciological observation sample

Direct annual glaciological observations are reported to the FoG database with their relative uncertainties in meters water equivalent (m w.e.) as:

$$B_{glac} \pm \sigma_{B_{glac}} \quad (1)$$

In the cases where a glaciological series is missing an uncertainty estimate for a given year, we assume it to be equal to the mean of all valid annual uncertainty estimates within the series. In the cases where glaciological series have no uncertainty estimate for the entire period, we assume it to be equal to the mean annual uncertainty for all glaciological series from glaciers belonging to the same region.

From the individual glacier annual glaciological time series, we estimate an individual glacier annual anomaly as the glaciological mass change value at year Y minus the mean mass change during the reference period from 2011 and 2020. Choosing a recent reference period allows to select a larger glaciological sample, thus getting a better representativity of glacier temporal variabilities across all regions. We allow a threshold of at least 8 years of glaciological observations within the 10-year reference period to calculate a glacier annual anomaly.

$$\beta_Y = B_{glac,Y} - \bar{B}_{glac,2011-2020} \quad (2)$$

Starting from a given glacier g belonging to the RGI 6.0 glacier inventory (e.g. Hintereisferner in Fig. 2), we use the sample of neighboring glacier anomalies to capture the temporal variability of its mass changes. First, we perform a spatial search of nearby glacier annual anomalies $(\beta_{i,Y})$ in five radial distance steps of 60, 120, 250, 500 and 1000 km from the glacier center point (Fig. 2a). To ensure a good representativeness of the temporal variability of the glacier, more than two glacier anomalies need to be selected. The spatial search stops at the distance where this condition is met. In case no individual glacier annual anomalies are found within the 1000 km threshold, glacier anomalies from the same or neighboring RGI 1st order regions are selected manually following Table 2. The mean annual anomaly of glacier g $(\overline{\beta}_{g,Y})$ is then calculated inverse distance weighted average of the spatially-selected sample of N individual glacier annual anomalies located nearby the glacier (Fig. 2b).

$$\overline{\beta}_{g,Y} = \frac{1}{N}\sum_{i=1}^{N} \beta_{i,Y} \cdot W_d \quad (3)$$

Where $W_d = \left(\frac{1}{d}\right)^{0.5}$ corresponds to the inverse distance weight, and d is the distance from glacier I to glacier g. The mean annual anomaly uncertainty is then calculated from the combination of two independent sources of error: First, the mean uncertainty inherited from the spatially-selected glaciological sample. In the case where glaciological series ire missing an uncertainty estimate for a given year, we assume it to be equal to the mean of all valid annual uncertainty estimates within the series. In the case where a glaciological series has no uncertainty estimate, we assume it to be equal to the mean annual uncertainty for all glaciological series from glaciers belonging to the same region. Secondly, we consider the variability of the individual spatially-selected annual glacier anomalies, measured as two times the standard error. In other words, the standard

https://doi.org/10.5194/essd-2024-323
Preprint. Discussion started: 12 August 2024

deviation of the N spatially-selected annual glacier anomalies over the common period, divided by the number of observations (n_Y) at the given year. This allows years with less observations to get larger errors than years having a larger observation sample. These two errors are then combined according to the law of random error propagation.

$$\sigma_{\bar{\beta}_{g,Y}} = \sqrt{\bar{\sigma}_{B_{glac,Y}}{}^2 + \sigma_{var_{\beta_Y}}{}^2} \qquad (4)$$

Where, $\bar{\sigma}_{B_{glac,Y}} = \frac{1}{N}\sum_{i=1}^{N} \sigma_{B_{glac,i,Y}}$ is the simple average from the glaciological sample uncertainties

and $\sigma_{var_{\beta_Y}} = 2 \cdot \frac{1}{\sqrt{n_Y}}\sum_{i=1}^{N} Stdev\ \beta_i$

We removed low confidence glaciological series from the FoG database. In the under sampled regions Arctic Canada South, Russian Arctic, Asia South East, Asia South West and New Zealand, we added complementary glacier anomalies from neighbouring regions to calculate the mean glacier anomalies (Table 2). As a rule, all glaciers mean annual-anomalies should cover at least the period between the hydrological years from 1976 to 2023. For glaciers with mean annual-anomalies not arriving back to 1976, the best correlated glaciological series from neighboring regions (i.e. climatically similar) are used to fill in the gap years only (Table 2, Zemp et al., 2019, 2020; Braithwaite and Hughes, 2020; Fernández and Somos-Valenzuela, 2022). To reduce the effect of possible climatic differences within the neighbouring regions, the amplitude of the complementary glacier anomalies is normalized to the amplitude of the mean glacier anomaly at the reference period.

Table 2: Regional overview of (i) Excluded glacier anomalies, (ii) complementary glacier anomalies added in under sampled regions to calculate the mean glacier anomalies, and (iii) complementary glacier anomalies, normalized and used on gap years only to extend the series back in time.

Region (number-RGI code)	**Excluded glacier anomalies**	**(ii) Complementary glacier anomalies**	**(iii) Complementary glacier anomalies** (Normalized)
02-WNA			Taku (ALA)
04-ACS		ACN anomalies	
05-GRL			Meighen and Devon Ice Caps (ACS)
06-ISL			Storbreen, Aalfotbreen and Rembesdalskaaka (SCA)
07-SJM			Storglacieren (SCA)
09-RUA		SJM anomalies	Storglacieren (SCA)
10-ASN	Hamagury yuki (ASN)		
11-CEU			Claridenfirn (CEU)
12-CAU			Hinteeisferner, Kesselwand (CEU)
13-ASC	Urumqi East and west branches (ASC)		
14-ASW		Ts. Tuyuksuyskiy (ASC)	
15-ASE		Ts. Tuyuksuyskiy, Urumqi (ASC)	
16-TRP	Yanamarey		Echaurren Norte (SAN-02)
17-SAN-01	All except Martial Este		Echaurren Norte (SAN-02)
17-SAN-02	All except Echaurren Norte		Echaurren Norte (SAN-02)

https://doi.org/10.5194/essd-2024-323
Preprint. Discussion started: 12 August 2024

18-NZL		Martial Este (SAN-01)	Echaurren Norte (SAN-02)
19-ANT	Dry valley glaciers		Echaurren Norte (SAN-02)

2.2.2. Calibrating the mean annual-anomaly on the glacier geodetic sample

Geodetic observations are reported to the FoG database with their relative uncertainties as mean rates of elevation change ($\frac{dh}{dt}$) in meters during a specific period of record (PoR). Glaciers may contain multiple individual geodetic observations for different time periods depending on the dates of the DEMs used (red and blue bars in Fig. 2c). To obtain the geodetic mass change rate, elevation changes need to be transformed to glacier specific mass change rates in m w.e. by applying a density conversion factor $f_\rho \pm \sigma_{f_\rho} = 0.85 \pm 0.60$ (Huss, 2013).

$$\bar{B}_{geo,PoR} = \overline{dh}_{PoR} \cdot f_\rho \qquad (5)$$

The geodetic mass change rate uncertainty is then calculated as the combination of two independent sources of error: the uncertainty related to the elevation change rate and the uncertainty related to the density conversion factor $\sigma_\rho = 60 kgm^{-3}$ (Huss, 2013). These two errors are combined according to the law of random error propagation as follows.

$$\sigma_{\bar{B}_{geo,PoR}} = \left|\bar{B}_{geo,PoR}\right| \sqrt{\left(\frac{\sigma_{\overline{dh}_{PoR}}}{\overline{dh}_{PoR}}\right)^2 + \left(\frac{\sigma_\rho}{f_\rho}\right)^2} \qquad (6)$$

In a data-fusion step, we calibrate the mean annual-anomaly (obtained from the glaciological sample) of glacier g to a given geodetic mass change rate k belonging to glacier g (i.e. geodetic sample). The k-calibrated mass change time series is then calculated as the sum of the geodetic mass change rate k and the mean annual-anomaly over the period of record of the geodetic mass change rate k (grey lines in Fig. 2c). Due to the large uncertainties related to the volume-to-mass-change conversion factor over short periods of time (Huss, 2013), only geodetic observations larger than 5 years are considered for calibration.

$$B_{cal,k,Y} = \bar{B}_{geo,k,PoR} + \left(\bar{\beta}_{g,Y} - \bar{\beta}_{g,PoR}\right) \qquad (7)$$

The k-calibrated mass change series uncertainty is then calculated as the combination of two independent errors: the uncertainty inherent to the individual geodetic mass change rates and the uncertainty inherited by the glacier's mean annual-anomaly. These two errors are combined according to the law of random error propagation.

2.2.3. Combining the resulting time series into a mean calibrated annual mass change time series

The mean calibrated annual mass change of glacier g (Fig. 2d) is finally calculated as the weighted mean of the K available k-calibrated time series (K is equal to the number of geodetic observations longer than 5 years available for the glacier). Two different weights are applied: First, a weight relative to the geodetic mass change uncertainty, where the k-calibrated series are weighted to the inverse ratio of the squared geodetic mass change rate uncertainty. And second, a weight relative to the time

https://doi.org/10.5194/essd-2024-323
Preprint. Discussion started: 12 August 2024

lag of the k-calibrated mass change time series in number of years to the initial (y_0) and final (y_1) years of the k geodetic rate PoR. Here, the point is to give more weight to a time series calibrated to a geodetic observation that is temporally close to the given geodetic PoR.

$$\bar{B}_{cal,g,Y} = \frac{\sum_{k=1}^{K} B_{cal,k,Y} \cdot W_{\sigma_{B_{geo,k,PoR}}} \cdot W_t}{K} \quad (8)$$

Where, $W_{\sigma_{\bar{B}_{geo,k,PoR}}} = \frac{1}{\sigma^2_{\bar{B}_{geo,k,PoR}}}$

and, $W_t = \left(\frac{1}{t_Y}\right)^{0.5}$ { $t = 1,\ y_0 < Y < y_1\ t = Y - y,\ Y > y_1\ t = y_0 - Y,\ Y < y$

For later error propagation, we separate the different source of errors of the mean calibrated time series $\bar{B}_{cal,g,Y}$, considering each source is entirely correlated with itself during the averaging of the different calibrated series. Based on previous equations, we separate errors from elevation change, density conversion and anomaly prediction:

$$\bar{\sigma}_{dh,\bar{B}_{cal,g,Y}} = \frac{1}{N}\sum_{k=1}^{N} \sigma_{\overline{dh}_{k,PoR}} \cdot f_\rho \quad (9)$$

$$\bar{\sigma}_{f_\rho,\bar{B}_{cal,g,Y}} = \frac{1}{N}\sum_{k=1}^{N} \sigma_{f_\rho} \cdot \overline{dh}_{k,PoR} \quad (10)$$

$$\bar{\sigma}_{\beta,\bar{B}_{cal,g,Y}} = \frac{1}{N}\sum_{k=1}^{N} \sigma_{\bar{\beta}_{k,Y}} \quad (11)$$

The mean calibrated time series total uncertainty for a certain glacier is:

$$\sigma^2_{\bar{B}_{cal,g,Y}} = \bar{\sigma}^2_{dh,\bar{B}_{cal,g,Y}} + \bar{\sigma}^2_{f_\rho,\bar{B}_{cal,g,Y}} + \bar{\sigma}^2_{\beta,\bar{B}_{cal,g,Y}} \quad (12)$$

2.2.4. Integrating glacier mass changes into larger regions

Every glacier with available geodetic observations has a mean-calibrated annual mass change (approximately 205.000 glaciers covering a 97.4% world's glaciated surface). The remaining unobserved glaciers (g_{unobs}) are assumed to behave as the regional mean of the observed sample. The Individual glacier mean-calibrated annual mass change time series can be integrated into any larger region R containing multiple glaciers. The regional (i.e. grid cell or glacier region) specific calibrated mass balance B_{cal} at year Y and in region R is calculated as the area weighted mean of the individual mean calibrated mass change time series of the sample of observed glaciers belonging to region R (or the specific grid point R for the gridded product, Fig 2e).

$$B_{cal,R,Y} = \frac{\sum_{g=1}^{N} \bar{B}_{cal,g,Y} \cdot A_g}{\left(\sum_{g=1}^{N} A_{g,Y}\right)} \quad (13)$$

To derive the uncertainty in the regional specific calibrated mass balance, we need to account for spatial correlations between the uncertainties of per-glacier calibrated mass balance. We identified three error sources that are significantly correlated spatially: elevation change, density conversion and annual anomaly prediction.

https://doi.org/10.5194/essd-2024-323
Preprint. Discussion started: 12 August 2024

For elevation change, we use the spatial correlation in elevation change error $\rho_{dh}(d)$ estimated in Hugonnet et al. (2021), as it is the main data source in the FoG database. These spatially correlated elevation errors are largely due to instrument noise and temporal interpolation to match an exact period of estimation.

$$\sigma^2_{dh,B_{cal,R,Y}} = \frac{1}{A_{tot}} \sum_{g_1} \sum_{g_2} \rho_{dh}(d_{g_1,g_2}) \cdot \sigma_{dh,\bar{B}_{cal,g_1,Y}} \cdot \sigma_{dh,\bar{B}_{cal,g_2,Y}} \cdot A_{g_1} \cdot A_{g_2} \quad (14)$$

where d_{g_1,g_2} is the distance between glaciers, A_g is the area of glacier g, and $A_{tot} = \sum_g A_g$ is the regional glacier area.

For density conversion, we use the spatial correlation in density conversion error $\rho_\rho(d)$ estimated by Huss et al. (in preparation). These spatially correlated density errors are largely due to large local and regional variations in precipitation and firn densification, resulting in spatially correlated errors from the average value.

$$\sigma^2_{f_\rho,B_{cal,R,Y}} = \frac{1}{A_{tot}} \sum_{g_1} \sum_{g_2} \rho_{f_\rho}(d_{g_1,g_2}) \cdot \sigma_{f_\rho,\bar{B}_{cal,g_1,Y}} \cdot \sigma_{f_\rho,\bar{B}_{cal,g_2,Y}} \cdot A_{g_1} \cdot A_{g_2} \quad (15)$$

For annual anomalies, we assume that errors to the real values are completely correlated at regional scales, and thus propagated as:

$$\sigma^2_{\beta,B_{cal,R,Y}} = \frac{1}{A_{tot}} \sum_g \sigma^2_{\beta,\bar{B}_{cal,g,Y}} \cdot A^2_g \quad (16)$$

Finally, we combine all sources of error propagated at the regional-scale as independent:

$$\sigma^2_{B_{cal,R,Y}} = \sigma^2_{dh,B_{cal,R,Y}} + \sigma^2_{f_\rho,B_{cal,R,Y}} + \sigma^2_{\beta,B_{cal,R,Y}} \quad (17)$$

The regional mass change in Gt of water is then obtained by multiplying the specific mass change by the region's (or grid point) glacierized area S_R (Fig 2f) accounting for area change. The regional total glacier mass change uncertainty is calculated from the combination of three independent errors: The error relative to the specific regional mass change, the error relative to the regional area (Paul et al., 2015) and the error relative to the area change. These three errors are combined according to the law of random error propagation.

$$\Delta M_{R,Y} = B_{R,Y} \cdot (S_R + \Delta S_{R,Y}) \quad (18)$$

$$\sigma_{\Delta M_{R,Y}} = |\Delta M_{R,Y}| \sqrt{\left(\frac{\sigma_{B_{R,Y}}}{B_{R,Y}}\right)^2 + \left(\frac{\sigma_{S_R}}{S_R}\right)^2 + \left(\frac{\sigma_{\Delta S_{R,Y}}}{\Delta S_{R,Y}}\right)^2} \quad (19)$$

Where $\frac{\sigma_S}{S} = 5\%$ (Paul et al., 2015) and $\frac{\sigma_{\Delta S_R}}{\Delta S_R}$ updated from Zemp et al. (2019)

The global annual (Y) and cumulative (PoR) mass change (in Gt) and sea level equivalent is finally calculated as the sum of the regional mass change, assuming that the regional mass loss uncertainties are independent and uncorrelated between every region.

$$\Delta M_{Glob,Y} = \sum_{R=1}^{19} \Delta M_{R,Y} \quad \text{and} \quad \Delta M_{Glob,PoR} = \sum_{R=1}^{19} \Delta M_{R,PoR} \quad (20)$$

https://doi.org/10.5194/essd-2024-323
Preprint. Discussion started: 12 August 2024

$$\sigma_{\Delta M_{Glob,Y}} = \sqrt{\sum_{R=1}^{19}\left(\sigma_{\Delta M_{R,Y}}\right)^2} \text{ and } \quad \sigma_{\Delta M_{Glob,PoR}} = \sqrt{\sum_{R=1}^{19}\left(\sigma_{\Delta M_{R,PoR}}\right)^2} \quad (21)$$

$$SLE_Y = \frac{\Delta M_{Glob,Y}}{S_{ocean}} \cdot 10^6 \pm \sigma_{SLE_Y} \quad \textit{and} \quad SLE_{PoR} = \frac{\Delta M_{Glob,PoR}}{S_{ocean}} \cdot 10^6 \pm \sigma_{SLE_{PoR}} \quad (22)$$

$$\sigma_{SLE_Y} = \sqrt{{\sigma_{\Delta M_{Glob,Y}}}^2 + {\sigma_{S_{ocean}}}^2} \quad \textit{and} \quad \sigma_{SLE_{PoR}} = \sqrt{{\sigma_{\Delta M_{Glob,PoR}}}^2 + {\sigma_{S_{ocean}}}^2} \quad (23)$$

Where $S_{ocean} = 362.5 \times 10^6 km^2$ and $\sigma_{S_{ocean}} = 0.1 \times 10^6 km^2$ (Cogley, 2012)

One strength of producing per-glacier mass change time series is the possibility to integrate them as an area-weighted mean at any given spatial resolution (i.e. regular grid, subregions, regions, basins, etc). In this study we integrate glacier mass changes in three spatial resolutions: Regionally by the 19 RGI 1st order regions and globally to allow direct comparison with previous global observation-based assessments by Zemp et al. (2019) and Hugonnet et al. (2021). Further, profiting from the per-glacier annual time series, we generate a global gridded product of annual glacier mass changes for the Copernicus Climate Change Service (C3S) Climate Data Store (CDS). For consistency with other climate observation datasets (e.g. C3S), we provide glacier changes at a global regular grid of 0.5° latitude longitude. For temporal consistency within all regions, we extend global time series only as far as the hydrological year 1976, in contrast to Zemp et al. (2019) who reached back to the 1960s. This adjustment is due to the absence of annual observations in the Southern Hemisphere regions prior to 1976 (evidenced in Fig. 7). Regional time series start from the date of the first year of mass change records available for the region (see Table 4). Importantly, our fully operational approach allows producing yearly updates as soon as new glacier observations are ingested into the FoG database of the WGMS.

2.2.5. Methodological progress in data fusion of glaciological and geodetic data

The specific methodological ameliorations on data fusion of glaciological and geodetic data of the present assessment with respect to Zemp et al. (2019) are detailed in Table 3.

Table 3: Specific methodological improvements in data fusion of glaciological and geodetic data with respect to Zemp et al. (2019)

	Zemp et al. (2019)	This study
Extraction of the temporal variability from the glaciological sample		
Selection strategy of glaciological time series	By spatial clusters defined from 1st and 2nd order regions	Automatically selected with respect to the distance to the glacier. Manual removal of

https://doi.org/10.5194/essd-2024-323
Preprint. Discussion started: 12 August 2024

		low confidence glaciological series from FoG WGMS,2024 (Table 2)
Combination strategy of glaciological anomalies	Variance decomposition model	Weighted by distance using a correlation function
Selection of complementary glacier anomalies from neighboring regions for under sampled cases	selected by arbitrary expert choice	Best correlated with regional time series (Table 2)
Normalized amplitude of the complementary glacier anomalies	No, used as is	Normalized to the amplitude of the regional series during the refence period (Table 2)
Calibration of the mean annual anomaly on the glacier geodetic sample		
Selection strategy of geodetic time series	All geodetic estimates available from FoG-WGMS, 2018 used	Removal of low confidence geodetic estimates from FoG WGMS,2024
Calibration strategy	Regional anomaly calibrated to geodetic rates of available observations, averaged per glacier and combined with estimates for sample without observations	Glacier anomaly calibrated over every individual geodetic rate and then combined by weighting mean considering geodetic uncertainty and distance to geodetic survey period
Uncertainty estimation and validation		
Time-dependent uncertainty accounting for area-change rates	Mean regional annual change rates	Mean regional annual change rates
Spatial correlation of uncertainties	Assuming uncorrelation for samples larger than 50 glaciers	Spatial Correlation following an empirical function Hugonnet et al, (2022), and Huss and Hugonnet (in prep)
Validation of results	Comparison with estimates in IPCC AR5	Leave-one-out Cross-validation over independent reference glacier time series
Special cases		
Special treatment in the Southern Andes region 17	Considered as a whole	Subdivided into two RGI 2nd order regions, Due to the scarcity of glaciological time series in the Southern Andes region and to better account for the distinct climatic conditions of the Central and Patagonian Andes (Garreaud, 2009; Garreaud et al., 2013)

https://doi.org/10.5194/essd-2024-323
Preprint. Discussion started: 12 August 2024

Correction of Echaurren Norte glaciological time series	Used as is	Past period (1976-2000) normalized with respect to present period amplitude due to suspicious values.

310

2.2.6. Description of the datasets

The datasets produced in this work are described in table 4. The main dataset, Dataset 1, corresponds to individual glacier annual mass change time series provided in .csv files by RGI first order regions. Glaciers are identified by their RGIId, centroid latitude and centroid longitude corresponding to the RGI60 glacier outline geometry. For Dataset 1, the start of the timeseries
315 is region-dependent and starts at the date of the first year of mass change records available for the region. The second Dataset 2 stands as a by-product from Dataset 1, it corresponds to an integration of the individual glacier timeseries a global regular grid of 0.5° latitude longitude. We chose this resolution and a netCDF file format to make the glacier change product consistent and easily usable by other climate observation datasets (e.g. C3S). To ensure global completeness of annual glacier mass changes, this dataset spans the period from 1976 to 2023.

320

Table 4. Details of the annual glacier mass change output datasets

	Dataset 1	**Dataset 2**
Dataset name	**Individual glacier annual mass change time series**	**Global gridded annual glacier mass changes**
Dataset access	Review process: https://user.geo.uzh.ch/idussa/Dussaillant_etal_ESSD_data/individual_glacier_annual_mass_change_time_series/ Upon publication: https://doi.org/10.5904/Dussaillant et al. YYYY-MM-DD	Review process: https://user.geo.uzh.ch/idussa/Dussaillant_etal_ESSD_data/global_gridded_annual_glacier_mass_changes/ Upon publication: https://doi.org/10.5904/Dussaillant et al. YYYY-MM-DD
File format	Coma delimited file (.csv) One file per RGI 1st order Region	NetCDF (.nc) One file per hydrological year
Data format	**Columns:** **RGIId:** glacier identifier from RGI60 (value of GLIMS_ID for Caucasus region 12) **CenLat:** glacier centroid Latitude extracted from the RGI60 glacier outline geometry. (GLIMS outlines for Caucasus region 12) **CenLon:** glacier centroid Longitude extracted from the RGI60 glacier outline geometry. (GLIMS outlines for Caucasus region 12) **YYYY:** Hydrological year named as last year of the hydrological cycle	**Variables :** Gacier change (Gt) Glacier change uncertainty (Gt) Glacier change (m w.e.) Glacier change uncertainty (m w.e.) Glacier area per grid point (km^2) **Dimensions:** Time Latitude Longitude **Grid point naming convention**: latitude, longitude at the middle of the grid point

https://doi.org/10.5194/essd-2024-323
Preprint. Discussion started: 12 August 2024

	Variable: glacier change time series and uncertainty in m w.e.	
Files names	**Mean calibrated mass change time series:** RRR_gla_mean-cal-mass-change-series.csv **Elevation change error:** RRR_ gla_mean-cal-mass-change_uncertainty_dh.csv **Annual anomaly error:** RRR_gla_mean-cal-mass-change_uncertainty_anom.csv **Density conversion error:** RRR_ gla_mean-cal-mass-change_uncertainty_rho.csv One file per RGI 1st order region, where RRR corresponds to the RGI-region code	**Mean calibrated mass change time series and total error:** global-gridded-annual-glacier-mass-change-YYYY.nc One file per hydrological year YYYY, named as last year of the hydrological cycle
Spatial Coverage	Global	Global
Spatial resolution	Individual glaciers	0.5° (latitude - longitude) regular grid
Temporal coverage	Time series start hydrological year is region dependent (see table XX) until hydrological year 2023	Hydrological years from 1976 to 2023
Temporal resolution	Annual, hydrological year	Annual, hydrological year
Conventions	n/a	NetCDF convention CF-1.8
Projection	Geographic Coordinate System: WGS 84 – EPSG:4326	Geographic Coordinate System: WGS 84 – EPSG:4326
Projection identifier	Centroid of glacier geometry (RGI60, GLIMS outlines for Caucasus, region 12)	Centroid of grid point

4. Results

4.1 Global glacier mass changes

Our results provide revised annual glacier mass changes extending back to the hydrological year 1975/76 at various spatial levels: per-glacier (Fig. 5 and 7), regional and on a global scale (Fig. 3, 4 and 5, Table 4). Globally, glaciers have lost 8226 ± 845 Gt of water (or 172 ± 27 Gt year^{-1}), contributing to 22.7 ± 2.3 mm of sea level rise since 1976. Almost half of the total loss (44%), equivalent to 10 mm of sea level rise was lost during the last decade from 2014-2023 only (Table 4).

https://doi.org/10.5194/essd-2024-323
Preprint. Discussion started: 12 August 2024

We find a record global mass loss for year 2023 with glaciers losing a total of 602 ± 69 Gt of water, the largest annual rates recorded (about 100 Gt larger than any other year on record) and the largest annual contribution to global mean sea level rise reported since 1976. In only one year, glacier melt contributed to raising the levels of the oceans by 1.7 mm. This corresponds to about 7% of the total sea level contribution of the last 5 decades from all the world's glaciers, lost in only one year. Strikingly, the global glacier mass loss curve follows an exponentially increasing loss slope during the past years, suggesting maintained and or increased glacier mass loss during the next years. Regionally, ice mean thickness losses during 2023 range from 0.5 m in the less impacted regions to up to 3.0 m in Western North America. Higher than average glacier mass loss was also reported in Alaska, Central Europe, the Southern Andes, High-Mountain Asia and New Zealand. Noteworthy four out of the last five years reported the highest global glacier mass in recorded history, with 2022 and 2023 as the first years where all glacier regions experienced ice loss.

https://doi.org/10.5194/essd-2024-323
Preprint. Discussion started: 12 August 2024

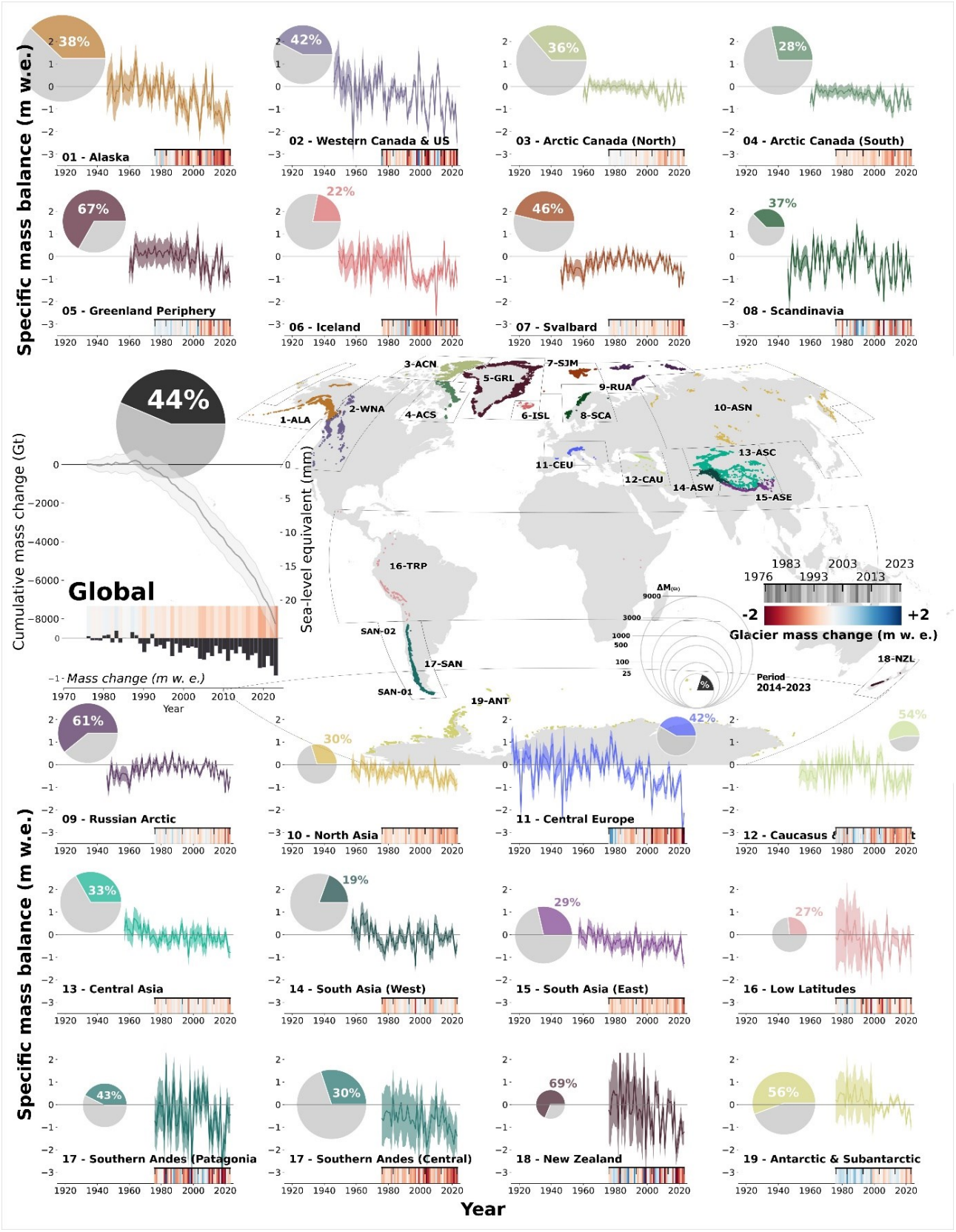

https://doi.org/10.5194/essd-2024-323
Preprint. Discussion started: 12 August 2024

Figure 3: Specific annual mass change time series for the 19 GTN-G regions (Southern Andes separated by 2nd Order RGI regions) with respective uncertainties. The area of the pie charts represents the mass lost (in Gt) by region and the globe since the hydrological year 1976. Colored sections represent the mass lost during the last decade (2014-2023). Heat maps represent regional and global glacier mass changes in m w.e. for every hydrological year over the common period from 1976 to 2023. Global results from 1976 to 2023 are represented both as specific mass change (bars and heat map) and as cumulative mass changes in (Gt). Regional time series start from the date of the first year of mass change records available for the region

4.2 Regional glacier mass changes

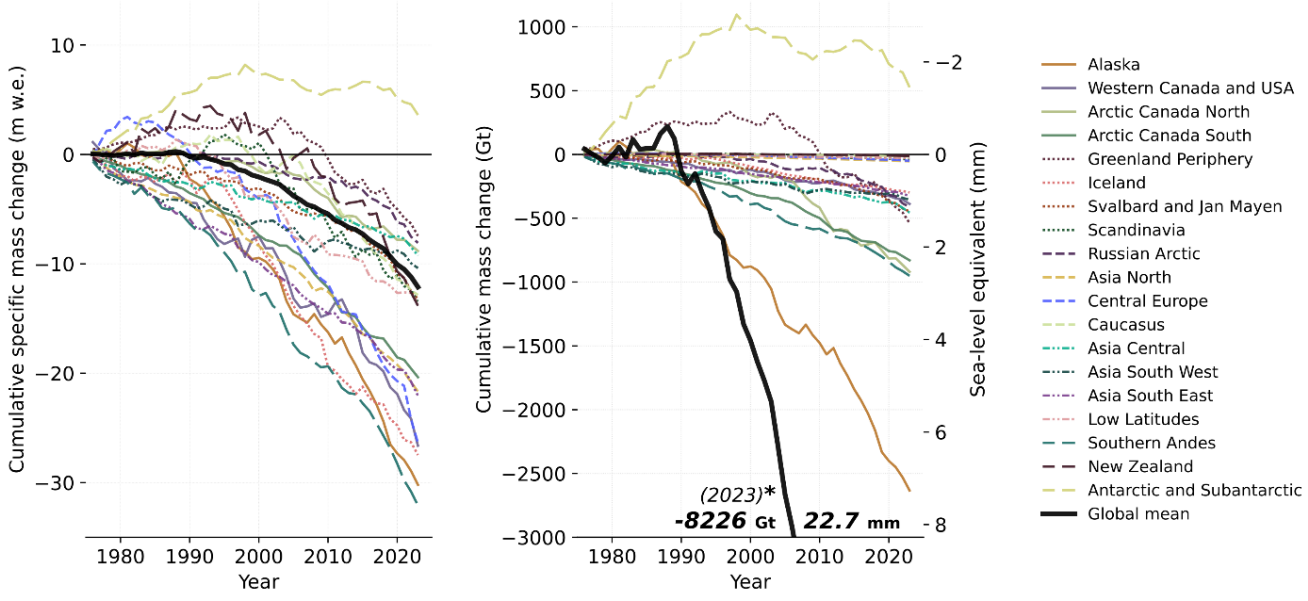

Figure 4: Cumulative regional glacier mass changes from hydrological year 1976 to present for the 19 GTN-G regions. Specific mass changes in m w.e. indicate the mean height of the water layer lost over a given glacier surface, large negative values suggest regions where glaciers have suffered the most. By multiplying by the regional glacier area in km^2 we obtain the mass-change in Gt of water. Cumulative glacier mass changes in Gt correspond to the volume of water lost (1 km^3 w.e. = 1 Gt) and are related to the regional contributions to global mean sea-level rise in mm.

During the last decades, all glacier regions have lost ice. Alaska, Western Canada US, Svalbard, Russian Arctic, North Asia, Caucasus, Central Asia, Asia East, Southern Andes, New Zealand and Antarctica have experienced increased mass loss during the last decade (2014-2023). Extremely negative regional decadal rates reaching down to -1.2 m w.e. yr^{-1} are observed in Alaska, Western North America and Central Europe during the last decade. Record-breaking annual rates (more negative than -2.5 m w.e.) occurred in Western North America (1958, 2023), Iceland (2010), the Central Andes (1999, 2018) and Central Europe with the largest and unprecedented regional annual rates reaching -3.1 m w.e. in 2022. Interestingly, the largest yearly total losses are not restricted to regions with the largest volumes, losses larger than 100 Gt in a single year are present in Antarctica (2012, and 2022), Greenland (2011) and Alaska (twelve years in total, five of them during the last decade) with two regional yearly record mass loss of 174 ± 45 Gt and 173 ± 42 Gt in 2004 and 2019 respectively. The ice lost during these 15

https://doi.org/10.5194/essd-2024-323
Preprint. Discussion started: 12 August 2024

specific years only (1834 ± 158 Gt) is equivalent to losing all the ice existing in Central Europe, Caucasus, Scandinavia, the Low Latitudes, New Zealand, North Asia and Western Canada together (total volume of 1690 ± 98 Gt in year 2000).

365

Table 4: Annual rates of regional glacier mass changes in Gt and m w.e. from 1976 to 2023 and the last decade from 2014 to 2023. Mean area is calculated from the annual changes in area estimated with change rates updated from Zemp et al. (2019).

GTN-G Region	Mean area (km^2) 1976-2023	Start hydrological year of time series	Mass change rate (Gt yr^{-1})		Mass change rate (m w.e. yr^{-1})	
			1976-2023	Last decade 2014-2023	1976-2023	Last decade 2014-2023
01 Alaska	90,507	1946	-54.9 ± 45.7	-99.5 ± 41.7	-0.63 ± 0.50	-1.20 ± 0.50
02 Western Canada US	15,045	1946	-8.1 ± 4.9	-16.4 ± 4.1	-0.55 ± 0.32	-1.21 ± 0.29
03 Arctic Canada North	105,119	1960	-19.2 ± 24.5	-33.4 ± 24.2	-0.18 ± 0.23	-0.32 ± 0.23
04 Arctic Canada South	40,892	1960	-17.3 ± 11.0	-23.5 ± 10.9	-0.42 ± 0.27	-0.58 ± 0.27
05 Greenland Periphery	89,978	1960	-11.2 ± 47.0	-35.9 ± 26.0	-0.16 ± 0.50	-0.48 ± 0.34
06 Iceland	11,080	1949	-6.2 ± 4.7	-6.6± 2.8	-0.57 ± 0.41	-0.64 ± 0.27
07 Svalbard	34,205	1946	-9.3 ± 7.1	-20.7 ± 5.7	-0.28 ± 0.20	-0.62 ± 0.17
08 Scandinavia	2,969	1946	-0.8 ± 0.9	-1.5 ± 0.8	-0.28 ± 0.31	-0.52 ± 0.30
09 Russian Arctic	51,965	1946	-8.6 ± 8.9	-25.1 ± 6.8	-0.17 ± 0.17	-0.50 ± 0.13
10 North Asia	2,529	1957	-1.1 ± 0.7	-1.6 ± 0.7	-0.45 ± 0.28	-0.69 ± 0.29
11 Central Europe	2,159	1915	-1.0 ± 0.6	-2.1 ± 0.5	-0.55 ± 0.29	-1.18 ± 0.27
12 Caucasus Middle East	1,317	1953	-0.3 ± 0.5	-0.9 ± 0.5	-0.27 ± 0.40	-0.71 ± 0.39
13 Central Asia	49,742	1957	-9.5 ± 17.6	-15.1± 13.0	-0.19 ± 0.35	-0.32 ± 0.27
14 South Asia West	33,849	1957	-7.4 ± 12.0	-6.9 ± 8.8	-0.22 ± 0.35	-0.22 ± 0.27
15 South Asia East	14,877	1957	-6.8 ± 4.9	-9.3 ± 3.6	-0.46 ± 0.32	-0.66 ± 0.25
16 Low Latitudes	2,335	1976	-0.6 ± 2.4	-0.8 ± 0.8	-0.28 ± 0.92	-0.42 ± 0.45
17 Southern Andes Patagonia	25,863	1976	-18.0 ± 26.5	-25.9 ± 20.8	-0.70 ± 1.02	-1.03 ± 0.83
17 Southern Andes Central	3,978		-1.9 ± 3.9	-3.4 ± 3.1	-0.47 ± 0.98	-0.98 ± 0.80
18 New Zealand	989	1976	-0.2 ± 1.1	-0.8 ± 0.4	-0.29 ± 1.11	-0.94 ± 0.52
19 Antarctic Subantarctic	129,100	1976	11.0 ± 92.0	-29.3 ± 20.9	-0.08 ± 0.69	-0.24 ± 0.17
GLOBAL	**708,498**	1976	**-172.4 ± 27.2**	**-358.9 ± 14.7**	**-0.25 ± 0.43**	**-0.54 ± 0.33**

https://doi.org/10.5194/essd-2024-323
Preprint. Discussion started: 12 August 2024

Open Access Earth System Science Data Discussions

5. Discussion

5.1 Multi-spatial dimensions of annual mass change series

The revised dataset claims several strengths, primarily related to the enhanced temporal resolution, providing glacier changes at annual resolution, and the multiple spatial dimensions for data integration from individual glacier to global. In a visualization example for selected years in Iceland, figure 5 depicts the multiple spatial dimensions from the dataset: Individual glacier annual time series (Fig. 5i) and annual time series aggregated into any larger scale region encompassing multiple glaciers, such as regular grid cells of 0.5-degree latitude longitude (e.g. Fig. 5ii or any user-specified resolution) and regional to global specific mass changes (Fig. 5iii and Fig. 3) and mass changes (Fig. 5iv, Fig. 8). This versatility enables identification of individual years marked by significant glacier changes and the detection of zones with varying impacts. For instance, it allows to pinpoint glaciers within a region that were affected by specific annual climate variations (e.g. droughts, floods, heat waves, etc.), as well as those with a larger or smaller influence on the yearly contribution to hydrology and annual sea level rise.

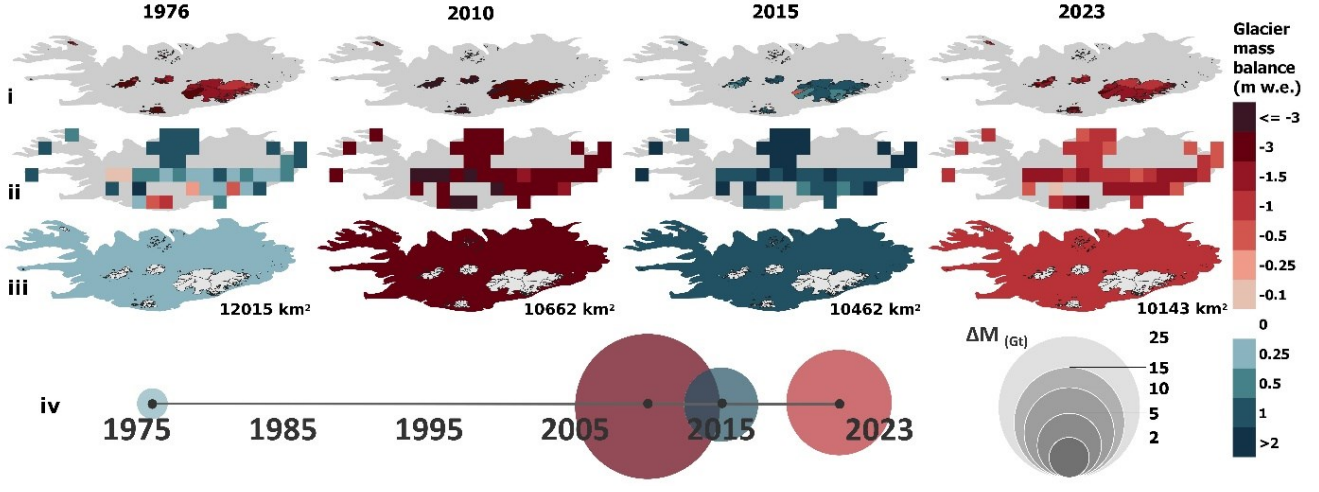

Figure 5: Illustration of the multi spatial dimensions of the global annual mass change series, example for the Iceland region during selected years. (i) Individual glacier annual mass change series, (ii) Gridded annual mass change series, (iii) Regional specific annual mass change in m w.e. and (vi) Regional mass change in Gt (note that all the previous dimensions i, ii and iii may also be represented in Gt).

Figure 5 illustrates the multidimensional characteristics of the global dataset in an example for region 6, Iceland. Represented years are chosen arbitrarily: the initial and last hydrological years considered in the global assessment, the well-known extremely negative mass change hydrological year 2010, attributed to the eruption of the Eyjafjallajökull volcano (Belart et al., 2019, 2020; Möller et al., 2019) and the most positive year of the series in 2015. This example allows to illustrate the rather homogeneous glacier mass loss of year 2010 with larger Icelandic glaciers all below -2 m w.e. and some smaller glacier between -1.5 and -2 m w.e., whereas other years show larger variabilities between glaciers and grid points. This example demonstrates the richness of the dataset for interpretation of glacier mass changes at different spatial scales and a deeper

https://doi.org/10.5194/essd-2024-323
Preprint. Discussion started: 12 August 2024

analysis of the spatial and temporal impact of known glaciological trends and anomalies like, for example, the Andes Megadrought (Gillett et al., 2006; Garreaud et al., 2017, 2020; Dussaillant et al., 2019) or the Karakoram anomaly (Farinotti et al., 2020; Gao et al., 2020; Ougahi et al., 2022) at an unprecedented yearly temporal resolution.

5.2 Leave-one-out cross validation

Due to the lack of independent measurements available to compare and validate our glacier change assessment, we applied a leave-one-out cross validation exercise over selected reference glaciers. The WGMS reference glaciers provide a reliable and well-documented sample of globally distributed long-term observation series with more than 30 years of continuous and ongoing glaciological mass-balance measurements. They are selected considering their fluctuations to be mainly driven by climatic factors, meaning they are not subject to other major influences such as avalanches, calving or surge dynamics, heavy debris cover, artificial snow production or melt protection. Further, the WGMS encourages periodically reanalyzing and calibration of the reference glaciers mass change series with results from high quality geodetic surveys to remove potential biases related to the glaciological method (Zemp et al., 2013). They thus represent excellent test sites for the validation of glaciological and geodetic data and related production methods. Here, 32 validated reference glacier time series are selected for cross-validation.

For each reference glacier, we compare the original reference mass change time series (Ba) as available from the FoG database, with its leave-one-out calibrated mass change time series (Leave-one-out Ba). The latter is obtained as described in the original methodology by calibrating the mean annual-anomaly of the reference glacier over its geodetic sample, only that this time we exclude the selected reference glacier anomaly from the processing. Reference glaciers are usually highly monitored and contain multiple sources of geodetic observations for different time periods. However, more than 80% of the world's glaciers present only one source of geodetic observations, i.e., the 20-year elevation change rates from the Hugonnet et al. (2021). To test the validity of our method over these under-sampled glaciers we only consider for calibration geodetic rates from Hugonnet et al. (2021). For each reference glacier, the Mean Absolute Error (MAE) and the Standard deviation of the difference (STDdiff) stand as a measure of the deviation of the calculated leave-one-out cross validation time series from the reference time series.

https://doi.org/10.5194/essd-2024-323
Preprint. Discussion started: 12 August 2024

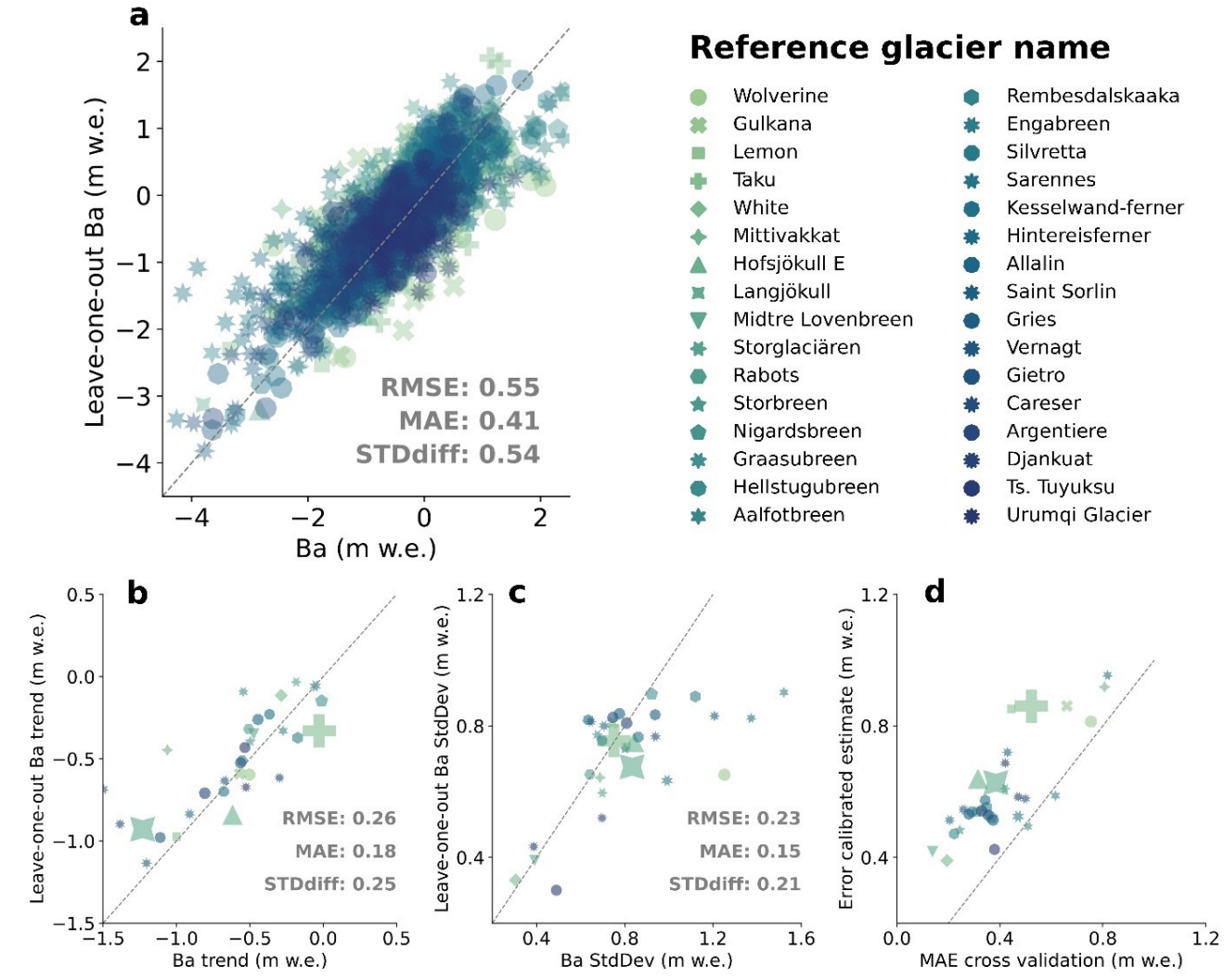

Figure 6: Leave-one-out cross-validation results and statistics. RMSE: Root Mean Square Error; MAE: Mean Absolute Error; STDdiff: Standard deviation of the difference between the calculated leave-one-out cross validation time series and the reference time series. (a) Leave-one-out calculated annual mass change (Ba) against the reference glaciers annual mass change observations. Every dot corresponds to one-year observation. (b) Leave-one-out calculated mass change standard deviation (i.e. amplitude of the annual variability) against reference glaciers mass change trends for the period 1976-2023 (c) Leave-one-out calculated mass change trends against reference glaciers mass change standard deviation for the period 1976-2023. (d) Reference glacier leave-one-out cross validation MAE against the estimated uncertainty of the mean calibrated estimate Ba calculated by our methodology for the same glacier. Symbols correspond to one of the 32 reference glaciers used for cross-validation. The size of the symbol is relative to the Area of the reference glacier.

Validation results are shown for all reference glaciers in Fig. 6. Considering all annual mass changes, we find a MAE of 0.41 and a STD-diff of 0.25 m w.e. of the calculated leave-one-out cross validation time series with respect to the reference time series. In general, regions with a rich glaciological sample, like the European Alps, Scandinavia, Svalbard, Iceland and Arctic

https://doi.org/10.5194/essd-2024-323
Preprint. Discussion started: 12 August 2024

Canada North perform well (Fig. 7 a-f). Hintereisferner located in the best sampled Central Europe region (mean anomaly estimated from seven glaciers within the 60 km range, Fig. 7a) presents a MAE of 0.2 m w.e. and a STD-diff of 0.24 m w.e.; On the contrary, glacier Gulkana in Alaska, presents larger MAE and STD-diff of 0.66 and 0.81 m w.e. respectively, with a mean anomaly estimated from only three distant glaciers (Fig. 7l). The remaining reference glacier statistics all lie between Hintereisferner and Gulkana, the best and worst-case scenarios, respectively.

We find no systematic error for Ba (Fig 6a, 7), verified by the equivalent RMSE and STD-diff of the leave-one-out cross validation residuals for all reference glaciers. This means there are only random errors generated by our method. Differences in the long-term trends (MAE 0.18 m w.e., Fig 6b) may come from the different geodetic datasets used for calibration. Reference glacier mass change series should undergo reanalysis and calibration with high quality, local and long-term geodetic estimates, while our methodology combines all geodetic estimates available for the glacier by weighting their trends (see methods).

Some glaciers show a slight tendency towards underestimated extreme values of Ba variability, which amplitude is expressed by the StdDev (Fig 6c). Notably in Afoltbreen most of the negative (most positive) years in the reference Ba series are estimated as less negative (less positive) in the Leave-one-out Ba (Fig 7g). This effect is clearly represented by the slight shift towards smaller standard deviations of the mass change series with respect to the reference series (Fig. 6c). This bias may come from a slight smoothing of the mean annual-anomaly extreme values when averaging the nearby glaciological times series. Our cross-validation results show this bias to be well accounted for in the uncertainty assessment, still we note there is room for improvement of the algorithm in this aspect.

The calculated error of the reference glaciers observational calibrated mass change series ($\sigma_{\bar{B}_{cal,g,Y}}$) is on average 0.2 m w.e. larger than the cross-validation MAE (Fig. 6d), confirming that our uncertainty estimation is within an acceptable range and can capture sources of systematic errors or random errors introduced by the prediction method. We can conclude that the spatial extrapolation based on the mean-anomaly calibration, on average, does not introduce new systematic errors and has a per-glacier random error that is well represented based on the sample of reference glacier. The leave-one-out cross validation results prove that our algorithm can capture the annual variability of individual glacier mass changes on glaciers not presenting glaciological time series (99% of the global glaciers). It is anyways important to note that reference glaciers are, in general, located in regions where there are often other series to compensate for their exclusion. Due to this, the leave-one-out analysis does not necessarily represent a typical glacier in a data scarce region. Improvements in this aspect will only be reached with a better sample of long-term glacier mass balance time series in all glacier regions.

https://doi.org/10.5194/essd-2024-323
Preprint. Discussion started: 12 August 2024

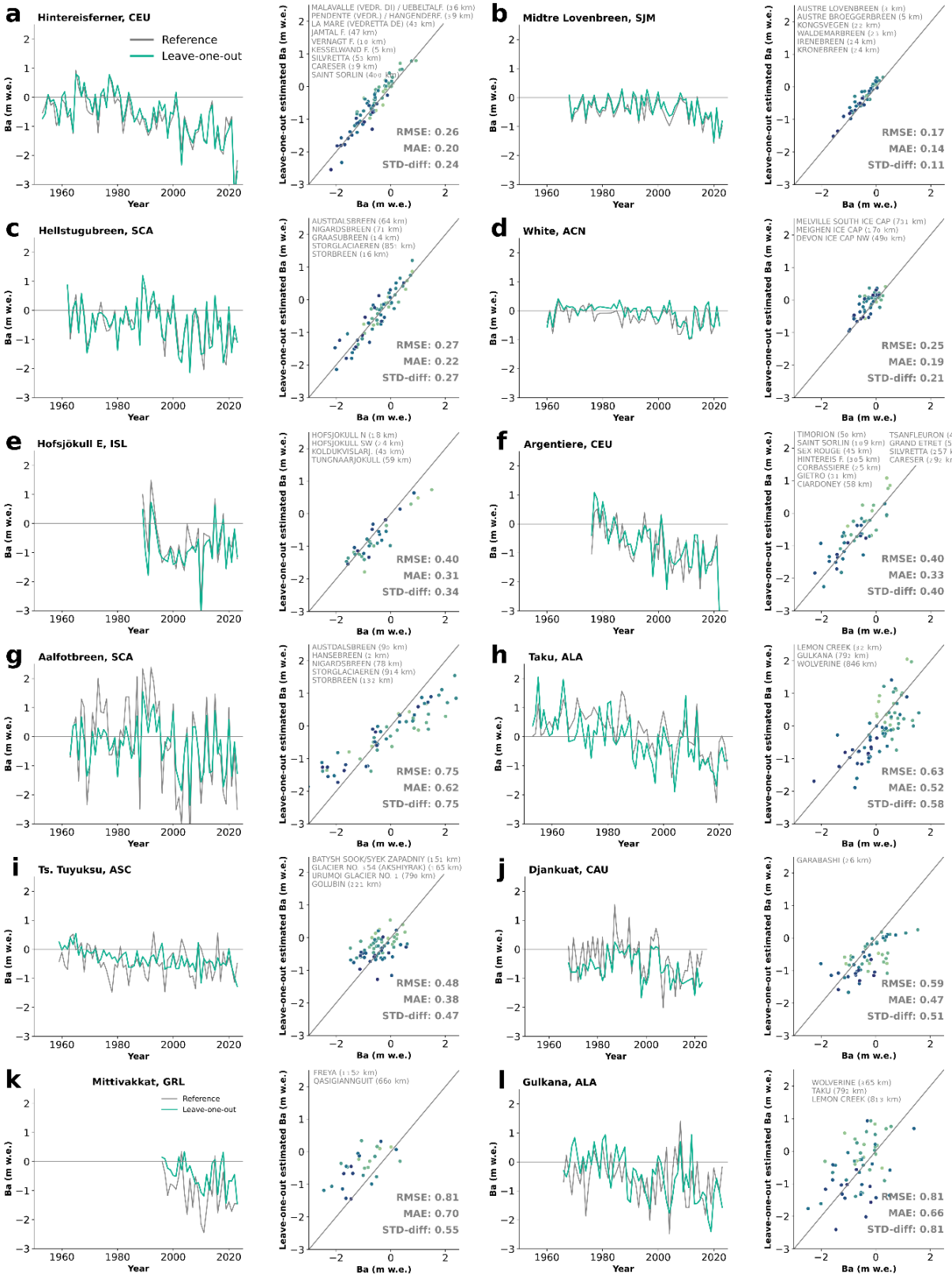

https://doi.org/10.5194/essd-2024-323
Preprint. Discussion started: 12 August 2024

Figure 7: Selected examples of the leave-one-out cross validation results by individual glaciers. (Right plots) Reference glacier annual mass change time series (grey) and the leave-one-out estimated annual mass change time series (blue). (Left plot) Annual mass change values from reference glaciers against the leave-one-out estimated annual mass change values. Every dot corresponds to a yearly observation. Nearby glaciers selected to calculate the zonal anomaly are listed together with their distance to the reference glacier.

5.4 Improvements with respect to earlier assessments

A general overview of the improvements with respect to both previous assessments from Zemp et al. (2019) and Hugonnet et al. (2021) is described in Table 5. Regional and global glacier mass change results for the three observation-based estimates are compared in Fig. 8 (in Gt).

Table 5: General methodological ameliorations with respect to Zemp et al. (2019) and Hugonnet et al. (2021)

	Zemp et al. (2019)	Hugonnet et al. (2021)	This study
Spatial coverage	9%	97.4% of glacier area	96% of glacier area
Spatial resolution	GTN-G Region	Individual glaciers RGI-6	Individual glaciers RGI-6 Regular global grid
Temporal coverage	1960 – 2016 (with global annual resolution 1976 – 2016)	2000 - 2020	1976 – 2023 Globally (regionally <1976, see table 4)
Temporal resolution	annual	Multi annual (5,10 and 20 years)	annual
Uncertainty sources for individual glaciers time series	N/A (only regional time series)	**σ dh** **σ density** mean (Huss, 2013)	**σ dh** **σ density** mean (Huss, 2013) **σ glac. anomaly**
Uncertainty sources regional time series	**σ dh** and **σ glac** propagated assuming uncorrelation for samples larger than 50 glaciers **σ density** mean (Huss, 2013) **σ area change rate** from regional annual mean	**σ dh** propagation (Hugonnet et al, 2022)	**Empirical spatial correlation function** **σ dh** propagation (Hugonnet et al, 2022) **σ glac anomaly** propagation **σ density** propagation (Huss and Hugonnet (in prep)) **σ area change rate** from regional annual mean
Annual updates	No update	Not updated yet	Yearly updated since 2022 (C3S CDS)
Glacier inventory Caucasus region 12	RGI-6	GLIMS	GLIMS

https://doi.org/10.5194/essd-2024-323
Preprint. Discussion started: 12 August 2024

Broadly, our new approach effectively corrects the negative bias in the long-term trends observed in Zemp et al. (2019) thanks to the integration of the glacier elevation changes by Hugonnet et al. (2021), which translates into a significant reduction in both regional and global uncertainties, largely noticeable for the more recent years (Fig.8). Globally, glacier mass change rates between 1976 and 2016 are less negative (-131.6 ± 28 Gt yr^{-1}) than previously estimated by Zemp et al. (2019) (-203.8 ± 45.4 Gt yr^{-1}, Table 6). The resulting 5394 Gt of cumulative mean mass loss for the period is 58% from that predicted by Zemp et al. (2019) (9290 Gt). The differences mainly come from Alaska, Antarctic and Subantarctic Islands, Greenland Periphery, and the Russian Arctic (Table 6) – all regions with limited geodetic coverage, as already pointed out by Zemp et al. (2019). Both regionally and globally, the years after 2000 are well aligned to the Hugonnet et al. (2021) trends as consequence of the calibration to their geodetic trends with global coverage.

Larger deviation in regional trends are noticeable over regions holding limited geodetic samples during the Zemp et al. (2019) assessment, i.e. covering less than 50% of the regional area with valid observations. More specifically, Alaska, Arctic Canada North, Western North America, the Russian Arctic, Caucasus, Low Latitudes, New Zealand and the Southern Andes exhibit less negative general trends. In contrast, the trends in the Asia North region are more negative, and Arctic Canada South more negative in the past. Overall, the regional trends agree well with Hugonnet et al. (2021) trends during the overlapping period 2000-2019 (Table 6). Deviations of more than 5 Gt yr^{-1} are found in Alaska, Greenland Periphery, and Antarctic and Subantarctic Islands.

https://doi.org/10.5194/essd-2024-323
Preprint. Discussion started: 12 August 2024

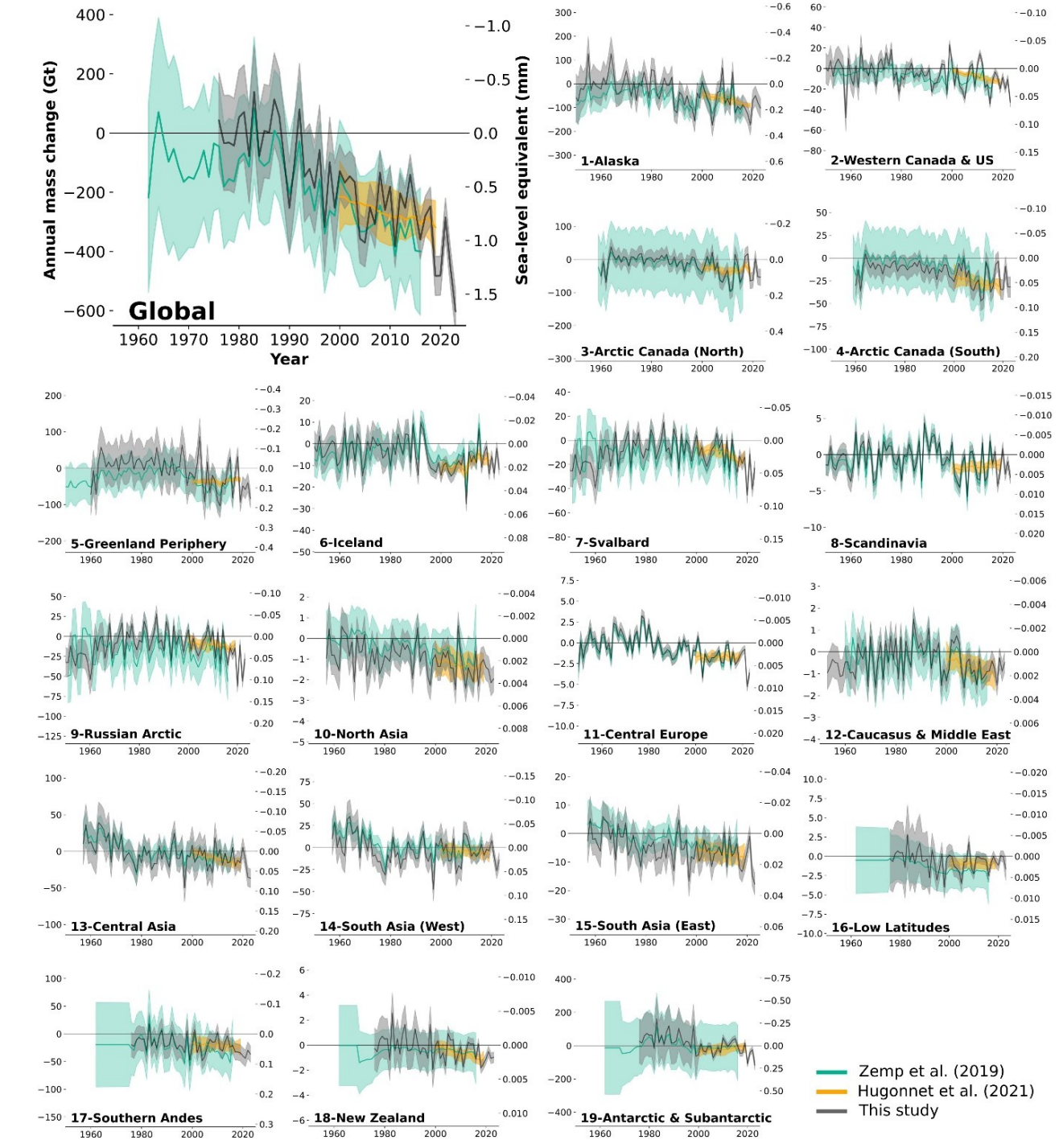

https://doi.org/10.5194/essd-2024-323
Preprint. Discussion started: 12 August 2024

Figure 8: Annual glacier mass change (Gt) from this study compared with results from Zemp et al. (2019) and Hugonnet et al. (2021).

Strong deviations remain in the Greenland Periphery and Antarctic and Subantarctic Islands regions during the past period, where our trend results are considerably less negative than in Zemp et al. (2019). Difference in Greenland can be explained by the removal of unpublished geodetic observations from our processing chain, which may have overfitted the trends in Zemp et al. (2019). The new calibrated mass change time series relies on the 2000-2019 Hugonnet et al. (2021) and 1985-2000 Huber et al. (2020) as calibration reference for the present and past periods respectively. The Antarctic and Subantarctic Islands is a region prone to large uncertainties in all mentioned studies. Even though they agree within (large) uncertainties, our results show slightly larger mass gain trends of 21.7 ± 99.2 Gt $year^{-1}$ compared to the 5.5 ± 152.0 Gt $year^{-1}$ from Zemp et al. (2019) for the 1976-2016 period. Conversely, slightly less negative mass change of -10.7 ± 21.2 Gt $year^{-1}$ are observed compared to -20.9 ± 4.9 Gt $year^{-1}$ for Hugonnet et al. (2021) during 2000-2019. Differences with Hugonnet et al. (2021) trends may come from the different regional geodetic sample considered, i.e. elevation change rates for 535 glaciers (4% of the glacier area in this RGI region 19) from Hugonnet et al. (2021) were not included in the FoG database, and therefore in this assessment, due to their lack of coverage in the elevation change maps (less than 50%). Further, the Antarctic and Subantarctic Islands region presents no glaciological or geodetic measurements before the year 2000. The signal for the past annual variability (before 2000) is driven purely by the very-distant Echaurren Norte normalized time series, and past trends are only calibrated over the 2000-2019 Hugonnet et al. (2021) series, which are very likely overfitting the period before 2000 towards more positive values. There is insufficient evidence to support the glacier mass gain observed before 2000 in both our assessment and the Zemp et al. (2019). We assume results in the Antarctic region to be very likely biased by the lack of observations, and therefore highly uncertain, as reflected in our large error bars. However, we still include them to provide global glacier mass changes back to 1976. Hence, the global mass changes in Gt represent an upper bound for the period before 2000 due to the large weight of the Antarctic and Subantarctic Islands region (18% of the global glaciated surface).

Most regions display increased amplitudes in their interannual variability when compared to both previous studies. The Gaussian regression used to fit the DEM time series in Hugonnet et al. (2021) has a smoothing effect on the annual amplitude to the point where annual variability is no longer detected (Fig.8). Similarly in Zemp et al. (2019), the variance decomposition model (Eckert et al., 2011; Krzywinski and Altman, 2014) employed to extract the temporal mass change variability for each region has shown to contribute to a slight smoothing of the annual amplitude signal (Zemp et al., 2020). Our approach allows to better represent the glacier interannual amplitude at the individual glacier level, supported by the Leave-one-out cross validation exercise (Fig. 6c and 7) and the effect is inherited to the regional and global level.

https://doi.org/10.5194/essd-2024-323
Preprint. Discussion started: 12 August 2024

Importantly, our assessment reduces global and regional uncertainties compared to Zemp et al. (2019) (Table 4). This reduction is achieved firstly, because our approach benefits from the almost complete-observational sample from Hugonnet et al. (2021) as calibration, which highly reduces uncertainties after year 2000. Thirdly, multiple algorithm improvements, such as the spatial search of glacier anomalies, the normalization of neighbouring glacier time series with original regional amplitudes. Notably, considering error propagation using empirical functions for the different sources of error provides more realistic uncertainties than previous work. All these enhancements are further supported by the leave-one-out-cross validation over reference glaciers, confirming that our uncertainties remain still on the conservative side. Compared with Hugonnet et al. (2021), results agree within uncertainties, but our estimated errors are consistently larger throughout all regions. This is coming from the propagation of the mean-anomaly uncertainties, which are the larger source of error in our assessment, and a source that was not considered in the Hugonnet et al. (2021) annual results.

Our approach provides corrected absolute trends of glacier mass change with reduced uncertainties for individual glaciers, regions and the globe. One of the largest strengths of the method is the ability to provide glacier mass changes back in time up to 1976 at a global level and even further back in regions with longer observational records (e.g. 1915 for Central Europe). Noteworthy, we can capture the annual temporal variability of glacier changes at the per-glacier level with realistic uncertainty estimation. By combining the strengths of the two previous global observation-based assessments, we improve both the spatial resolution and the temporal variability of global glacier mass changes, allowing to produce a new gridded product of annual glacier changes based purely on observations.

Table 6: Annual rates of regional glacier mass change for the period 1976-2016 from this study compared with results from Zemp et al. (2019) for the same period and annual rates of regional glacier mass change for the period 2000-2019 from this study compared with results from Hugonnet et al. (2021) for the same period. Mean area is calculated from the annual changes in area estimated with change rates updated from Zemp et al. (2019).

GTN-G Region	Mean area (km^2) (1976-2016)	Mass change ($Gt\ year^{-1}$)		Mean area (km^2) (2000-2019)	Mass change ($Gt\ year^{-1}$)	
		This study (1976-2016)	Zemp et al. (2019) (1976-2016)		This study (2000-2019)	Hugonnet et al. (2021) (2000-2019)
01 Alaska	91,980	-47.0 ± 46.3	-65.2 ± 41.0	86,299	-72.3 ± 43.5	-66.7 ± 10.9
02 Western Canada US	15,303	-7.0 ± 5.0	-9.6 ± 10.0	14,311	-9.6 ± 4.1	-7.6 ± 1.7
03 Arctic Canada North	105,387	-17.4 ± 24.5	-24.5 ± 92.0	104,354	-31.7- ± 24.2	-30.5 ± 4.8
04 Arctic Canada South	40,996	-16.5 ± 11.1	-9.6 ± 32.0	40,594	-22.2 ± 10.9	-26.5 ± 4.3
05 Greenland Periphery	92,409	-5.6 ± 49.7	-24.9 ± 46.0	83,464	-29.2 ± 38.5	-35.5 ± 5.8
06 Iceland	11,219	-5.9 ± 4.9	-3.9 ± 6.0	10,681	-9.2 ± 3.2	-9.4 ± 1.4
07 Svalbard	34,372	-6.8 ± 7.2	-13.2 ± 12.0	33,767	-10.7 ± 5.8	-10.5 ± 1.7
08 Scandinavia	2,997	-0.7 ± 1.0	-0.9 ± 1.0	2,889	-1.7 ± 0.9	-1.7 ± 0.4

https://doi.org/10.5194/essd-2024-323
Preprint. Discussion started: 12 August 2024

09 Russian Arctic	52,219	-5.0 ± 9.2	-20.0 ± 24.0	51,300	-10.6 ± 6.8	-10.4 ± 1.9
10 North Asia	2,565	-1.0 ± 0.7	-0.5 ± 1.0	2,426	-1.3 ± 0.7	-1.3 ± 0.4
11 Central Europe	2,227	-0.8 ± 0.7	-1.0 ± 1.0	1,966	-1.6 ± 0.6	-1.7 ± 0.4
12 Caucasus Middle East	1,342	-0.3 ± 0.6	-0.5 ± 1.0	1,248	-0.6 ± 0.5	-0.7 ± 0.2
13 Central Asia	50,237	-8.0 ± 18.3	-5.9 ± 15.0	48,327	-8.3 ± 18.5	-9.6 ± 2.1
14 South Asia West	34,173	-7.3 ± 12.5	-1.9 ± 10.0	32,924	-4.5 ± 12.6	-4.6 ± 1.7
15 South Asia East	15,034	-6.1 ± 5.1	-3.2 ± 5.0	14,428	-6.9 ± 4.3	-6.9 ± 1.4
16 Low Latitudes	2,430	-0.6 ± 2.6	-1.5 ± 3.0	2,069	-0.8 ± 0.9	-0.9 ± 0.2
17 Southern Andes	30,009	-17.1 ± 19.5	-22.8 ± 40.0	29,420	-21.4 ± 15.5	-20.7 ± 4.1
18 New Zealand	1,017	-0.1 ± 1.2	-0.4 ± 2.0	909	-0.5 ± 0.6	-0.7 ± 0.2
19 Antarctic & subantarctic	130,356	21.7 ± 99.2	5.5 ± 152.0	125,513	-10.7 ± 21.2	-20.9 ± 4.9
GLOBAL	**716,272**	**-131.6 ± 28.8**	**-203.8 ± 45.4**	**686,889**	**-253.7 ± 16.5**	**-267 ± 8.0**

5.3 Known limitations

5.3.1. Scarcity of the glaciological in-situ observations

The scarcity of glaciological data stands as the primary limitation in assessing the variability of glacier changes with our methodology. In sparsely observed regions like High Mountain Asia, the Southern Andes, Arctic Canada South, the Russian Arctic, Greenland and Antarctica, annual variations in glacier changes depend on limited and distant regional or neighboring regions timeseries, which may not necessarily be representative of the local glacier annual variability. As consequence, the annual glacier mass change time series exhibit high uncertainties in these regions, realistically estimated by our method.

We note a significant observational gap in the Southern Hemisphere where the glacier mass change variability before 2000 is driven by the single and very distant Echaurren Norte glacier time series. This provokes a massive overrating of its importance at the global scale. The best way forward while still maintaining the independence and observation-based nature of the present assessment -crucial for calibration and validation of glacier models- is to bolster in-situ glacier monitoring programs in these regions. In the short term, efforts must be directed towards ensuring the continuity of glacier in situ monitoring in the Southern Hemisphere and possible correction of past long-term series.

5.3.1. Availability of past geodetic observations

The lack of geodetic observations for the period before 2000 is consistent for most glacier regions, and critical for accurate results of our assessment in less sampled regions, as shown for the Antarctic and Subantarctic Islands. The best way to correct possible deviations in past time series is to calibrate them against accurate long-term geodetic glacier elevation changes. Geodetic observations can be temporally enriched in all regions by unlocking historical spy satellite archives (e.g. Hexagon, Corona) and national historical airborne image archives.

https://doi.org/10.5194/essd-2024-323
Preprint. Discussion started: 12 August 2024

5.3.2. Grid point artifact in polar regions

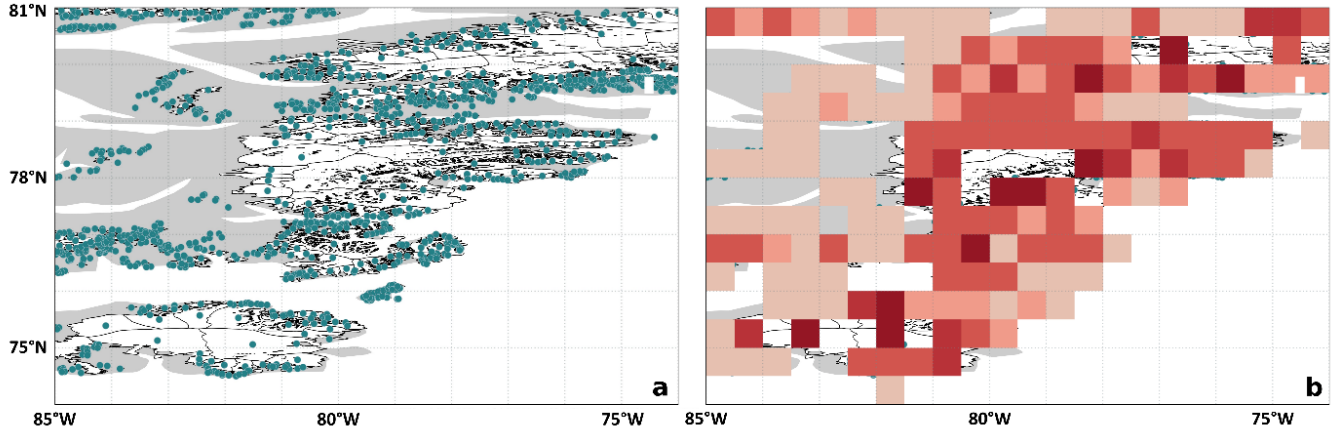

Figure 9: Mockup example of the grid point artifact in polar regions. (a) Glacier outlines (white) and their centroids (blue points) in the region Arctic Canada North under 1° grid cells. (b) Illustration of how the 0.5° gridded mass balance integration looks like.

To assess glacier mass changes, it is imperative to treat a glacier as a unified and indivisible entity. A sound glaciological approach for integrating glacier-wide changes into a regular grid system is to consider a glacier belonging to a grid point if its centroid falls within that grid point's boundaries. If the grid cell is sufficiently large, it will encompass multiple glaciers at their full extension within the grid cell and the grid-point mean mass change will be determined accordingly. However, in cases where the grid cell is smaller than the glacier's surface area, the grid point containing the glacier's centroid will represent the mass change of the entire glacier, despite not all its extension is contained within the grid point (Fig. 8a). This discrepancy is particularly evident in polar regions above 60° latitude when integrating mass changes at a 0.5° global grid resolution. Polar grid points are relatively smaller in surface area compared to the large polar glaciers. Consequently, this leads to a biased estimate of mass change at the grid point containing the glaciers centroid and consequent neighboring glacierized grid points lack a mass change estimate (see Figure 9b).

This issue might be especially critical for deconvolving the glacier signal for Gravimetry or other applications in polar regions due to coarse resolution of the ancillary datasets (usually not smaller than 0.5°). A potential solution for larger scale applications with coarser spatial resolution would be an area-weight per tile glacier area, but this would bring an additional bias related to the divisibility of the glacier signal.

5.3.3. Calendar years vs hydrological years

Our results present regional glacier mass changes spanning the hydrological years from 1976 to 2023. In glaciological terms, it is widely accepted that the hydrological year starts in winter with the onset of the accumulation season and concludes at the end of the summer or ablation season (Cogley et al., 2011). Consequently, the hydrological year varies across regions (South

https://doi.org/10.5194/essd-2024-323
Preprint. Discussion started: 12 August 2024

and North Hemispheres and Tropics) and does not align to the calendar year. Gridded annual glacier mass change values for a given hydrological year will not be fully consistent. For grid-points located in the northern hemisphere glacier mass changes correspond to the period from the 1st October of the previous year to 30th September of the given year. Whereas grid-points in the southern hemisphere will represent glacier mass changes from the 1st April of the previous year to 31st March of the given year. It is important to note that this discrepancy, stemming from the input data, introduces inconsistencies and uncertainties on the gridded global assessments that users should acknowledge. For cumulative values over longer periods, these differences become less significant. Addressing this issue would need an increase in temporal resolution of the input data to monthly observations, which is not feasible at the global level purely relying on observations.

5.3.4 Glacier specific area-change rates

We consider the impact of glacier area changes in time for our regional mass change estimates as done by Zemp et al. (2019). In the former study, the evolution of area change rates is calculated for each first-order glacier region independently represented in two-time steps: a past period with no change rates and then a linear change rate calculated from a regional sample of glaciers with observations. This assumption is strong since glacier area changes are far from being linear, still is the best possible guess considering the available observations. In this study, we further assume the glacier specific area-change rates behave as their regional mean change rates. This may introduce an additional bias since glacier specific area change rates strongly depend on the size of the considered glaciers, with an observed decreasing mean and increasing variability of relative area changes towards smaller glaciers (Paul, 2004; Fischer et al., 2014). This also implies that the average change obtained for a greater region ultimately depends on the glacier size distribution considered in a specific sample, which may or may not be representative of the full regional glacier size range present in the RGI60 inventory used here.

6. Data availability

The annual mass change time-series for individual glaciers and the derived global gridded annual mass change product at a spatial resolution of 0.5° latitude and longitude will be made available with the publication of this article from the World Glacier Monitoring Service (https://doi.org/10.5904/ Dussaillant et al. 2024-MM-DD). During the review process, the data is temporarily available from URL: https://user.geo.uzh.ch/idussa/Dussaillant_etal_ESSD_data/. Earlier versions of the gridded product are available from the Copernicus Climate Data Store (CDS) web-based service (Dussaillant et al. 2023, DOI 10.24381/cds.ba597449). The present version will follow in the next C3S phase. FoG database version used here (WGMS, 2024; https://doi.org/10.5904/wgms-fog-2024-01) is available for download from the WGMS website (https://wgms.ch/data_databaseversions/). RGI version 6.0 is available from the National Snow and Ice Data Center (NSIDC, RGI consortium 2017; https://doi.org/10.7265/4m1f-gd79).

7. Code availability

https://doi.org/10.5194/essd-2024-323
Preprint. Discussion started: 12 August 2024

615 The code is available at https://github.com/idussa/mb_data_crunching. We aim to publish the final version at the end of the review process.

8. Conclusions

Building on the strengths and insights from previous global observation-based assessments of glacier mass change, we present a novel integrated approach that provides globally comprehensive, per-glacier annual mass changes and their associated
620 uncertainties from 1976 to 2023. Our results offer critical insights into the alarming acceleration of glacier melt, revealing significant contributions to global sea level rise, particularly evident in the last decade and specifically in 2023 with a record loss of 602 ± 69 Gt. Over the past five decades, glaciers globally have lost 8226 ± 845 Gt (171 ± 27 Gt year^{-1}) of water contributing to a 22.7 ± 2.3 mm (0.5 ± 0.3 mm year^{-1}) rise in sea levels. Nearly half (44%) of this loss occurred in the last decade, with 7% occurring in 2023 alone.

625 Compared to earlier assessments, our new dataset allows to extend annual glacier change observations across five decades. By integrating extensive geodetic data, our approach corrects existing biases in long-term trends and enables to estimate the interannual variability of mass changes at an individual glacier level, improving both the spatial and temporal resolution of previous global glacier mass change assessments while maintaining the dataset's independence and purely observational nature. Validation through a leave-one-out cross-validation exercise confirms the dataset's ability to capture the interannual variability
630 of individual glacier mass changes with realistic uncertainty estimates.

The primary limitation of this assessment is the scarcity of glaciological observations, particularly regions with sparse and widely spaced mass change time series. Consequently, the mean anomalies of annual glacier changes captured may not accurately reflect the local variability in under-sampled regions. While refining the climatic regions used to capture mean anomalies could enhance accuracy, substantial improvements ultimately depend on larger glaciological samples. Therefore,
635 ensuring the continuation of local in-situ monitoring efforts is crucial for sustaining and updating global glacier mass change assessments. Support should be directed towards regions with a low density of in-situ measurements, often coinciding with countries facing resource limitations or situated in highly remote areas. Moreover, maintaining spaceborne missions for cryosphere observation proves to be essential for preserving the global completeness and long-term accuracy of glacier changes worldwide.

640 Glaciers are classified as one of the Earth's Essential Climate Variables (ECV, GCOS, 2022). This assessment provides new empirical evidence on the evolution of glaciers at local, regional, and global scales, to guide mitigation and adaptation measures related to a changing cryosphere. The refined data underscores the urgent need for global climate action to understand and adapt to the adverse effects of accelerated glacier melting and its cascading impacts on environmental systems. Our results,

https://doi.org/10.5194/essd-2024-323
Preprint. Discussion started: 12 August 2024

freely available through the WGMS and the C3S CDS, hold vast potential for applications in various fields within and beyond glaciology. These include international cryosphere observation intercomparison exercises; multi-Essential Climate Variable (ECV) products; serving as invaluable resources for calibrating and validating climate models; and advancing our understanding of the broader implications of glacier melt on sea levels, freshwater resources, global energy budgets, and nutrient cycling. This work opens new opportunities for future assessments of global glacier mass changes at increased temporal resolutions, fostering a more detailed examination of their climate and hydrological impacts worldwide.

Author contribution

I.D. and M.Z. initiated and coordinated the study. I.D. compiled the data, performed all the processing and analysis, wrote the manuscript and produced all figures. R.H. supported the uncertainty assessment algorithm. J.B. supported as project manager for the Copernicus Climate Change Service data product. All authors supported the analysis and commented on the manuscript.

Competing interests

The contact author has declared that none of the authors has any competing interests

Acknowledgements

The present method was developed within the World Glacier Monitoring Service and the Global Gravity based Groundwater product (G3P) project as contributions to G3P, The Glacier Mass Balance Intercomparison Exercise (GlaMBIE) and the Copernicus Climate Change Service Climate Data Store (C3S-CDS)

References

Abermann, J., Fischer, A., Lambrecht, A., and Geist, T. (2010). On the potential of very high-resolution repeat DEMs in glacial and periglacial environments. *The Cryosphere* 4, 53–65. doi: 10.5194/tc-4-53-2010

Arendt, A. A. (2002). Rapid Wastage of Alaska Glaciers and Their Contribution to Rising Sea Level. *Science* 297, 382–386. doi: 10.1126/science.1072497

Belart, J. M. C., Magnússon, E., Berthier, E., Gunnlaugsson, Á. Þ., Pálsson, F., Aðalgeirsdóttir, G., et al. (2020). Mass Balance of 14 Icelandic Glaciers, 1945–2017: Spatial Variations and Links With Climate. *Frontiers in Earth Science* 8. doi: 10.3389/feart.2020.00163

Belart, J. M. C., Magnússon, E., Berthier, E., Pálsson, F., Aðalgeirsdóttir, Gu., and Jóhannesson, T. (2019). The geodetic mass balance of Eyjafjallajökull ice cap for 1945–2014: processing guidelines and relation to climate. *Journal of Glaciology*, 1–15. doi: 10.1017/jog.2019.16

https://doi.org/10.5194/essd-2024-323
Preprint. Discussion started: 12 August 2024

Berthier, E., Floricioiu, D., Gardner, A. S., Gourmelen, N., Jakob, L., Paul, F., et al. (2023). Measuring Glacier Mass Changes from Space - A Review. *Reports on Progress in Physics* 86, 036801. doi: 10.1088/1361-6633/acaf8e

Braithwaite, R. J., and Hughes, P. D. (2020). Regional Geography of Glacier Mass Balance Variability Over Seven Decades 1946–2015. *Frontiers in Earth Science* 8. doi: 10.3389/feart.2020.00302

Braun, M. H., Malz, P., Sommer, C., Farías-Barahona, D., Sauter, T., Casassa, G., et al. (2019). Constraining glacier elevation and mass changes in South America. *Nature Climate Change* 9, 130. doi: 10.1038/s41558-018-0375-7

Brun, F., Berthier, E., Wagnon, P., Kääb, A., and Treichler, D. (2017). A spatially resolved estimate of High Mountain Asia glacier mass balances from 2000 to 2016. *Nature Geoscience* 10, 668–673. doi: 10.1038/ngeo2999

Cogley, J. G., and Adams, W. P. (1998). Mass balance of glaciers other than the ice sheets. *J. of Glaciology* 44, 315–325. doi: 10.3189/S0022143000002641

Cogley, J. G., Hock, R., Rasmussen, L. A., Arendt, A. A., Bauder, A., Braithwaite, R. J., et al. (2011). *Glossary of Glacier Mass Balance and Related Terms*., IHP-VII Technical Documents in Hydrilogy No. 86. IACS Contribution No. 2 UNESCO-IHP, Paris.

Dehecq, A., Millan, R., Berthier, E., Gourmelen, N., Trouve, E., and Vionnet, V. (2016). Elevation Changes Inferred From TanDEM-X Data Over the Mont-Blanc Area: Impact of the X-Band Interferometric Bias. *IEEE Journal of Selected Topics in Applied Earth Observations and Remote Sensing*, 1–13. doi: 10.1109/JSTARS.2016.2581482

Dussaillant, I., Berthier, E., Brun, F., Masiokas, M., Hugonnet, R., Favier, V., et al. (2019). Two decades of glacier mass loss along the Andes. *Nat. Geosci.* 12, 802–808. doi: 10.1038/s41561-019-0432-5

Echelmeyer, K. A., Harrison, W. D., Larsen, C. F., Sapiano, J., E, M. J., Mallie, J. D., et al. (1996). Airborne surface profiling of glaciers: a case-study in Alaska. *Journal of Glaciology* 42, 538–547. doi: 10.3189/S002214300000352X

Eckert, N., Baya, H., Thibert, E., and Vincent, C. (2011). Extracting the temporal signal from a winter and summer mass-balance series: application to a six-decade record at Glacier de Sarennes, French Alps. *Journal of Glaciology* 57, 134–150. doi: 10.3189/002214311795306673

Farinotti, D., Immerzeel, W. W., de Kok, R. J., Quincey, D. J., and Dehecq, A. (2020). Manifestations and mechanisms of the Karakoram glacier Anomaly. *Nat. Geosci.* 13, 8–16. doi: 10.1038/s41561-019-0513-5

Fernández, A., and Somos-Valenzuela, M. (2022). Revisiting glacier mass-balance sensitivity to surface air temperature using a data-driven regionalization. *Journal of Glaciology* 68, 1041–1060. doi: 10.1017/jog.2022.16

Finsterwalder, R. (1954). Photogrammetry and Glacier Research with Special Reference to Glacier Retreat in the Eastern Alps *. *Journal of Glaciology* 2, 306–315. doi: 10.3189/S0022143000025119

Fischer, M., Huss, M., Barboux, C., and Hoelzle, M. (2014). The New Swiss Glacier Inventory SGI2010: Relevance of Using High-Resolution Source Data in Areas Dominated by Very Small Glaciers. *Arctic, Antarctic, and Alpine Research* 46, 933–945. doi: 10.1657/1938-4246-46.4.933

Gao, H., Zou, X., Wu, J., Zhang, Y., Deng, X., Hussain, S., et al. (2020). Post-20th century near-steady state of Batura Glacier: observational evidence of Karakoram Anomaly. *Sci Rep* 10, 987. doi: 10.1038/s41598-020-57660-0

https://doi.org/10.5194/essd-2024-323
Preprint. Discussion started: 12 August 2024

Gardelle, J., Berthier, E., Arnaud, Y., and Kääb, A. (2013). Region-wide glacier mass balances over the Pamir-Karakoram-Himalaya during 1999–2011. *The Cryosphere* 7, 1263–1286. doi: 10.5194/tc-7-1263-2013

Gardner, A. S., Moholdt, G., Cogley, J. G., Wouters, B., Arendt, A. A., Wahr, J., et al. (2013). A Reconciled Estimate of Glacier Contributions to Sea Level Rise: 2003 to 2009. *Science* 340, 852–857. doi: 10.1126/science.1234532

Garreaud, R. D. (2009). The Andes climate and weather., in *Advances in Geosciences*, (Copernicus GmbH), 3–11. doi: https://doi.org/10.5194/adgeo-22-3-2009

Garreaud, R. D., Alvarez-Garreton, C., Barichivich, J., Boisier, J. P., Christie, D., Galleguillos, M., et al. (2017). The 2010–2015 megadrought in central Chile: impacts on regional hydroclimate and vegetation. *Hydrol. Earth Syst. Sci.* 21, 6307–6327. doi: 10.5194/hess-21-6307-2017

Garreaud, R. D., Boisier, J. P., Rondanelli, R., Montecinos, A., Sepúlveda, H. H., and Veloso-Aguila, D. (2020). The Central Chile Mega Drought (2010–2018): A climate dynamics perspective. *International Journal of Climatology* 40, 421–439. doi: 10.1002/joc.6219

Garreaud, R., Lopez, P., Minvielle, M., and Rojas, M. (2013). Large-Scale Control on the Patagonian Climate. *Journal of Climate* 26, 215–230. doi: 10.1175/JCLI-D-12-00001.1

Gillett, N. P., Kell, T. D., and Jones, P. D. (2006). Regional climate impacts of the Southern Annular Mode. *Geophys. Res. Lett.* 33, L23704. doi: 10.1029/2006GL027721

Girod, L., Nuth, C., Kääb, A., McNabb, R. W., and Galland, O. (2017). MMASTER: Improved ASTER DEMs for Elevation Change Monitoring. *Remote Sensing* 9, 704. doi: 10.3390/rs9070704

GTN-G (2017). GTN-G Glacier Regions. doi: 10.5904/gtng-glacreg-2017-07

Hagg, W. J., Braun, L. N., Uvarov, V. N., and Makarevich, K. G. (2004). A comparison of three methods of mass-balance determination in the Tuyuksu glacier region, Tien Shan, Central Asia. *Journal of Glaciology* 50, 505–510. doi: 10.3189/172756504781829783

Huber, J., McNabb, R., and Zemp, M. (2020). Elevation Changes of West-Central Greenland Glaciers From 1985 to 2012 From Remote Sensing. *Frontiers in Earth Science* 8, 1–16. doi: 10.3389/feart.2020.00035

Hugonnet, R., Brun, F., Berthier, E., Dehecq, A., Mannerfelt, E. S., Eckert, N., et al. (2022). Uncertainty Analysis of Digital Elevation Models by Spatial Inference From Stable Terrain. *IEEE Journal of Selected Topics in Applied Earth Observations and Remote Sensing* 15, 6456–6472. doi: 10.1109/JSTARS.2022.3188922

Hugonnet, R., McNabb, R., Berthier, E., Menounos, B., Nuth, C., Girod, L., et al. (2021). Accelerated global glacier mass loss in the early twenty-first century. *Nature* 592, 726–731. doi: 10.1038/s41586-021-03436-z

Huss, M. (2013). Density assumptions for converting geodetic glacier volume change to mass change. *The Cryosphere* 7, 877–887. doi: 10.5194/tc-7-877-2013

Jakob, L., and Gourmelen, N. (2023). Glacier Mass Loss Between 2010 and 2020 Dominated by Atmospheric Forcing. *Geophysical Research Letters* 50, e2023GL102954. doi: 10.1029/2023GL102954

Joerg, P. C., and Zemp, M. (2014). Evaluating Volumetric Glacier Change Methods Using Airborne Laser Scanning Data. *Geografiska Annaler: Series A, Physical Geography* 96, 135–145. doi: 10.1111/geoa.12036

https://doi.org/10.5194/essd-2024-323
Preprint. Discussion started: 12 August 2024

Kaser, G., Fountain, A., and Jansson, P. (2003). A manual for monitoring the mass balance of mountain glaciers by. *IHPVI Technical documents in Hydrology* 2003, 135.

Krzywinski, M., and Altman, N. (2014). Analysis of variance and blocking. *Nature Methods* 11, 699–700. doi: 10.1038/nmeth.3005

Letréguilly, A., and Reynaud, L. (1990). Space and time distribution of glacier mass-balance in the Northern Hemisphere. *Arctic and Alpine Research*, 43–50.

McNabb, R., Nuth, C., Kääb, A., and Girod, L. (2019). Sensitivity of glacier volume change estimation to DEM void interpolation. *The Cryosphere* 13, 895–910. doi: https://doi.org/10.5194/tc-13-895-2019

Menounos, B., Hugonnet, R., Shean, D., Gardner, A., Howat, I., Berthier, E., et al. (2019). Heterogeneous Changes in Western North American Glaciers Linked to Decadal Variability in Zonal Wind Strength. *Geophysical Research Letters* 46, 200–209. doi: 10.1029/2018GL080942

Möller, R., Dagsson-Waldhauserova, P., Möller, M., Kukla, P. A., Schneider, C., and Gudmundsson, M. T. (2019). Persistent albedo reduction on southern Icelandic glaciers due to ashfall from the 2010 Eyjafjallajökull eruption. *Remote Sensing of Environment* 233, 111396. doi: 10.1016/j.rse.2019.111396

Nuth, C., and Kääb, A. (2011). Co-registration and bias corrections of satellite elevation data sets for quantifying glacier thickness change. *Cryosphere* 5, 271–290. doi: 10.5194/tc-5-271-2011

Oerlemans, J. (2001). *Glaciers and Climate Change*. CRC Press.

Østrem, G., and Brugman, M. M. (1991). Glacier mass-balance measurements: A manual for field and office work.

Ougahi, J. H., Cutler, M. E. J., and Cook, S. J. (2022). Assessing the Karakoram Anomaly from long-term trends in earth observation and climate data. *Remote Sensing Applications: Society and Environment* 28, 100852. doi: 10.1016/j.rsase.2022.100852

Papasodoro, C., Berthier, E., Royer, A., Zdanowicz, C., and Langlois, A. (2015). Area, elevation and mass changes of the two southernmost ice caps of the Canadian Arctic Archipelago between 1952 and 2014. *The Cryosphere* 9, 1535–1550. doi: https://doi.org/10.5194/tc-9-1535-2015

Paul, F. (2004). The new Swiss glacier inventory 2000 - Application of remote sensing and GIS. University of Zurich, Switzerland.

Paul, F., Bolch, T., Kääb, A., Nagler, T., Nuth, C., Scharrer, K., et al. (2015). The glaciers climate change initiative: Methods for creating glacier area, elevation change and velocity products. *Remote Sensing of Environment* 162, 408–426. doi: 10.1016/j.rse.2013.07.043

Pfeffer, W. T., Arendt, A. A., Bliss, A., Bolch, T., Cogley, J. G., Gardner, A. S., et al. (2014). The Randolph Glacier Inventory: a globally complete inventory of glaciers. *Journal of Glaciology* 60, 537–552. doi: 10.3189/2014JoG13J176

Raup, B. H., Kieffer, H. H., Hare, T. M., and Kargel, J. S. (2000). Generation of data acquisition requests for the ASTER satellite instrument for monitoring a globally distributed target: glaciers. *IEEE Transactions on Geoscience and Remote Sensing* 38, 8. doi: 10.1109/36.841989

https://doi.org/10.5194/essd-2024-323
Preprint. Discussion started: 12 August 2024

RGI Consortium (2017). Randolph Glacier Inventory - a dataset of global glacier outlines: version 6.0, technical report. Global Land Ice Measurements from Space, Colorado, USA. Digital Media. DOI: 10.7265/N5-RGI-60.

Rolstad, C., Haug, T., and Denby, B. (2009). Spatially integrated geodetic glacier mass balance and its uncertainty based on geostatistical analysis: application to the western Svartisen ice cap, Norway. *Journal of Glaciology* 55, 666–680. doi: 10.3189/002214309789470950

Rupnik, E., Daakir, M., and Pierrot Deseilligny, M. (2017). MicMac – a free, open-source solution for photogrammetry. *Open Geospatial Data, Software and Standards* 2, 14. doi: 10.1186/s40965-017-0027-2

Shean, D. E., Alexandrov, O., Moratto, Z. M., Smith, B. E., Joughin, I. R., Porter, C., et al. (2016). An automated, open-source pipeline for mass production of digital elevation models (DEMs) from very-high-resolution commercial stereo satellite imagery. *ISPRS Journal of Photogrammetry & Remote Sensing* 116, 101–117. doi: 10.1016/j.isprsjprs.2016.03.012

Shean, D. E., Bhushan, S., Montesano, P., Rounce, D. R., Arendt, A., and Osmanoglu, B. (2020). A Systematic, Regional Assessment of High Mountain Asia Glacier Mass Balance. *Frontiers in Earth Science* 7. Available at: https://www.frontiersin.org/article/10.3389/feart.2019.00363 (Accessed May 30, 2022).

Thibert, E., Blanc, R., Vincent, C., and Eckert, N. (2008). Glaciological and volumetric mass-balance measurements: error analysis over 51 years for Glacier de Sarennes, French Alps. *Journal of Glaciology* 54, 522–532. doi: 10.3189/002214308785837093

Thibert, E., and Vincent, C. (2009). Best possible estimation of mass balance combining glaciological and geodetic methods. *Annals Of Glaciology* 50, 112–118.

Thomson, L., Brun, F., Braun, M., and Zemp, M. (2021). Editorial: Observational Assessments of Glacier Mass Changes at Regional and Global Level. *Front. Earth Sci.* 8. doi: 10.3389/feart.2020.641710

Tielidze, L. G., and Wheate, R. D. (2018). The Greater Caucasus Glacier Inventory (Russia, Georgia and Azerbaijan). *The Cryosphere* 12, 81–94. doi: 10.5194/tc-12-81-2018

Toutin, T. (2001). Elevation modelling from satellite visible and infrared (VIR) data. *International Journal of Remote Sensing* 22, 1097–1125. doi: 10.1080/01431160117862

WGMS (2024). Fluctuations of Glaciers Database. doi: 10.5904/wgms-fog-2024-09

WMO, W. M. (2023). *Guide to Instruments and Methods of Observation. Volume II – Measurement of Cryospheric Variables*., 2023rd Edn. Available at: https://library.wmo.int/records/item/68660-guide-to-instruments-and-methods-of-observation (Accessed June 21, 2024).

Wouters, B., Gardner, A. S., and Moholdt, G. (2019). Global Glacier Mass Loss During the GRACE Satellite Mission (2002-2016). *Front. Earth Sci.* 7. doi: 10.3389/feart.2019.00096

Zemp, M., Frey, H., Gärtner-Roer, I., Nussbaumer, S. U., Hoelzle, M., Paul, F., et al. (2015a). Historically unprecedented global glacier decline in the early 21st century. *Journal of Glaciology* 61, 745–762. doi: 10.3189/2015JoG15J017

Zemp, M., Frey, H., Gärtner-Roer, I., Nussbaumer, S. U., Hoelzle, M., Paul, F., et al. (2015b). Historically unprecedented global glacier decline in the early 21st century. *Journal of Glaciology* 61, 745–762. doi: 10.3189/2015JoG15J017

https://doi.org/10.5194/essd-2024-323
Preprint. Discussion started: 12 August 2024

Zemp, M., Huss, M., Eckert, N., Thibert, E., Paul, F., Nussbaumer, S. U., et al. (2020). Brief communication: Ad hoc estimation of glacier contributions to sea-level rise from the latest glaciological observations. *The Cryosphere* 14, 1043–1050. doi: 10.3929/ethz-b-000408094

Zemp, M., Huss, M., Thibert, E., Eckert, N., McNabb, R., Huber, J., et al. (2019). Global glacier mass changes and their contributions to sea-level rise from 1961 to 2016. *Nature* 568, 382. doi: 10.1038/s41586-019-1071-0

Zemp, M., Thibert, E., Huss, M., Stumm, D., Rolstad Denby, C., Nuth, C., et al. (2013). Reanalysing glacier mass balance measurement series. *The Cryosphere* 7, 1227–1245. doi: 10.5194/tc-7-1227-2013